Stem Cell Reports
Article

OPEN ACCESS

Distinct Gene Expression and Epigenetic Signatures in Hepatocyte-like Cells Produced by Different Strategies from the Same Donor

Yimeng Gao,[1,8] Xiaoran Zhang,[2,8] Ludi Zhang,[1] Jin Cen,[1] Xuan Ni,[3] Xiaoying Liao,[3] Chenxi Yang,[4] Ying Li,[2] Xiaotao Chen,[1] Zhao Zhang,[1] Yajing Shu,[1] Xin Cheng,[1] David C. Hay,[5] Dongmei Lai,[6,9] Guoyu Pan,[3,9] Gang Wei,[2,*] and Lijian Hui[1,7,*]

[1]State Key Laboratory of Cell Biology, CAS Center for Excellence in Molecular Cell Science, Shanghai Institute of Biochemistry and Cell Biology, Chinese Academy of Sciences, University of Chinese Academy of Sciences, Shanghai 200031, China
[2]CAS Key Laboratory of Computational Biology, Collaborative Innovation Center for Genetics and Developmental Biology, CAS-MPG Partner Institute for Computational Biology, Shanghai Institutes for Biological Sciences, University of Chinese Academy of Sciences, Chinese Academy of Sciences, Shanghai 200031, China
[3]Center for Drug Safety Evaluation and Research, Shanghai Institute of Materia Medica, Chinese Academy of Sciences, Shanghai 201210, China
[4]State Key Laboratory of Bioreactor Engineering, School of Bioengineering, East China University of Science and Technology, Shanghai 200237, China
[5]MRC Centre for Regenerative Medicine, University of Edinburgh, Edinburgh EH16 4UU, UK
[6]The International Peace Maternity and Child Health Hospital, School of Medicine, Shanghai Jiaotong University, Shanghai 200030, China
[7]School of Life Science and Technology, ShanghaiTech University, Shanghai 201210, China
[8]Co-first author
[9]Co-senior author
*Correspondence: weigang@picb.ac.cn (G.W.), huilab@sibcb.ac.cn (L.H.)
https://doi.org/10.1016/j.stemcr.2017.10.019

SUMMARY

Hepatocyte-like cells (HLCs) can be generated through directed differentiation or transdifferentiation. Employing two strategies, we generated induced pluripotent stem cell (iPSC)-HLCs and hiHeps from the same donor cell line. Both types of HLCs clustered distinctly from each other during gene expression profiling. In particular, differences existed in gene expression for phase II drug metabolism and lipid accumulation, underpinned by H3K27 acetylation status in iPSC-HLCs and hiHeps. While distinct phenotypes were achieved *in vitro*, both types of HLCs demonstrated similar phenotypes following transplantation into Fah-deficient mice. In conclusion, functional HLCs can be obtained from the same donor using two strategies. Global gene expression defined the differences between those populations *in vitro*. Importantly, both HLCs displayed partial but markedly improved hepatic function following transplantation *in vivo*, demonstrating plasticity and the potential for cell-based modeling in the dish and cell-based therapy in the future.

INTRODUCTION

In order to overcome the limitations of using human hepatocytes from donor liver organs, methods to derive hepatocyte-like cells (HLCs) from other cells have been studied intensively (Forbes et al., 2015; Rezvani et al., 2016). To date, many different types of HLCs have been successfully generated from human pluripotent stem cells (hPSCs), with some derivative HLCs exhibiting respectable human drug metabolism and liver repopulation *in vivo* (Rezvani et al., 2016). hPSC-HLCs are typically obtained from hPSCs in a stage-wise process (Gerbal-Chaloin et al., 2014; Hay et al., 2008; Si-Tayeb et al., 2010; Sullivan et al., 2010; Touboul et al., 2010), whereas hiHeps are obtained by directing cellular transdifferentiation from human fibroblasts, or other cell types, by the forced expression of specific hepatocyte transcription factors (Du et al., 2014; Huang et al., 2014). To understand the advantages of both systems, a systemic comparison between induced pluripotent stem cell (iPSC)-HLCs and hiHeps is necessary to realize their translational value and understand the basic mechanisms that underpin hepatic differentiation and liver organogenesis (Forbes et al., 2015). While studies have been performed in PSCs, derived from the inner cell mass of nuclear transfer embryos, and iPSCs (Ma et al., 2014), a systematic study comparing iPSC-HLCs and hiHeps from the same donor has not been performed.

PSC-HLCs generated by different protocols were compared in a recent study (Godoy et al., 2015). On the basis of gene expression, gene networks were established to predict for successful or failed hepatocyte differentiation. In these studies, HNF1, FXR, and PXR were highlighted as key transcription factors required to improve HLC differentiation. In a similar approach, we have performed direct comparison of iPSC-HLC and hiHep gene expression and function *in vitro* and *in vivo*. This is of the utmost importance as iPSC-HLCs and hiHeps demonstrate significant potential in the quest to accurately model human disease and develop immune-matched cell-based therapies for the clinic (Bhatia et al., 2014; Fox et al., 2014). More specifically, our studies provide important information on the mechanisms that underlie cell identity changes during the process of liver differentiation and regeneration (Szkolnicka and Hay, 2016). Umbilical cord-derived fibroblasts (UCFs) were used in these studies. They were isolated from the same donor prior to reprogramming and directed differentiation or transdifferentiation, thereby removing the influence of genetic variation observed in the population

(Kajiwara et al., 2012). In summary, our studies focused on global gene expression and epigenetic remodeling to better understand the circuitry that underpins successful hepatic specification and cell function *in vitro* and *in vivo*.

RESULTS

Generation of Functional iPSC-HLCs and hiHeps from the Same Donor

Human umbilical cord fibroblasts, UCF1 and UCF2, were generated from two individuals (Figures S1A and S1B). The UCF donor cells were reprogrammed to iPSCs using standard methodology (Takahashi et al., 2007). The derivative iPSC lines were termed iPSC1 (derived from UCF1) and iPSC2 (derived from UCF2). Both lines expressed pluripotent stem cell markers (NANOG and SSEA4) and were positive for alkaline phosphatase (Figures S2A–S2D). In association with increased *OCT4* expression, the promoter of *OCT4* was demethylated (Figure S2E). After transplantation into the immune-deficient mice, both iPSC lines formed teratomas comprising tissues derived from the three germ layers (Figure S2F). Taken together, these results confirm that we produced two *bona fide* iPSC lines that could be maintained with normal karyotype for more than 40 passages (Figure S2G).

Both iPSC cells were differentiated into HLCs following a published protocol (Szkolnicka et al., 2014). We also transdifferentiated UCF1 and UCF2 into hiHep using *FOXA3*, *HNF1A*, and *HNF4A* as previously published (Huang et al., 2014) (Figure 1A). To confirm cell identity, hiHeps and iPSC-HLCs were validated to be genetically identical with the parental lines by short tandem repeat typing (Table S1). Morphologically, both hiHeps and iPSC-HLCs displayed typical epithelial phenotype, forming tight junctions, and canaliculi monolayers became confluent (Figure 1B). Interestingly, the diameter of the iPSC-HLCs was approximately 25% larger than that of hiHeps (12.6 μm in hiHeps versus 15.8 μm in iPSC-HLCs). A more detailed analysis demonstrated that the expression levels of typical hepatic markers were comparable between hiHeps and iPSC-HLCs, and those approached the levels detected in primary human hepatocytes (PHHs) as determined by qPCR (Figure 1C). Hepatocellular specification was also monitored by flow cytometry, and around 80% hiHeps and iPSC-HLCs co-expressed ALBUMIN and α-1-antitrypsin (AAT) (Figure 1D). The expression and secretion of ALBUMIN and AAT were further confirmed by ELISA, using supernatants from iPSC-HLCs and hiHeps. Of note, both proteins were detected at levels comparable with that in PHH cultures (Figure S3A). These data together indicate that iPSC-HLC and hiHep cells were homogeneous populations displaying typical hepatocyte features.

Differential Hepatocyte Gene Expressions in iPSC-HLCs and hiHeps

Following our initial characterization, we preformed genome-wide profiling of iPSC-HLCs and hiHeps and compared their gene expression (Table S2) with UCFs and PHHs controls. The top 4,000 most variably expressed genes between UCFs and PHHs that cultured for 1, 2, and 4 days were selected for further analysis. Whole-genome analysis using principal component analysis (PCA) confirmed that iPSC-HLCs, hiHeps, UCFs, and PHHs were clustered into distinct groups (Figure 2A).

Following this, we focused our analyses on differential gene expression between iPSC-HLCs and hiHeps. Unsupervised clustering of hepatic genes was performed, following with gene ontology enrichment analysis (Figures 2B and 2C). Based on the different gene expression patterns of hiHeps, iPSC-HLCs, and PHHs, the highly expressed hepatic genes could be divided into seven clusters. Genes involving fat digestion and absorption (e.g., *FABP1*, *APOB*) and metabolism enzymes (e.g., *GPX3* and *ACOX1*) were enriched in cluster I; their expression was induced in both hiHeps and iPSC-HLCs. There were some hepatic genes showing low expression in both iPSC-HLCs and hiHeps (cluster IV), including cytochrome P450-based metabolism genes (e.g., *CYP2C9*, *CYP2E1*, and *CYP3A4*) and coagulation complements (e.g., *F5*, *F9*, and *F11*).

Genes in cluster II were highly expressed in hiHeps but not in iPSC-HLCs. For example, the phase II metabolic enzymes (e.g., *UGT1A1* and *UGT1A6*) and ABC transporters (e.g., *ABCC2* and *ABCB1*) were highly enriched in cluster II genes. The expression of genes in cluster III was induced in iPSC-HLCs, and included fat digestion and absorption genes (e.g., *APOA2* and *FASN*) and bile secretion genes (e.g., *OATPB* and *NTCP*) (Figure 2C). Moreover, in clusters V, VI, and VII, the typical fibrotic genes and pathways were downregulated in HLCs (Figure S4A). Taken together, these studies highlighted differential gene expression between iPSC-HLCs and hiHeps.

Comparison of hiHep and iPSC-HLC Function *In Vitro*

Whole-genome analyses of expression profiles elucidated differences between iPSC-HLCs and hiHeps. To understand its functional implications, we measured several key hepatic functions in both cell types. As highlighted from gene expression analyses, both cells carried comparable levels of glycogen storage abilities as determined by periodic acid-Schiff (PAS) staining and colorimetric assay (Figures 3A and 3B).

To investigate phase I cytochrome P450 (CYP) induction, we treated hiHeps and iPSC-HLCs with 3-methylcholanthrene, phenobarbital, and rifampicin. hiHeps and iPSC-HLCs also possessed remarkable capacities to respond to these chemicals (Figures S3B and S3C). We specifically

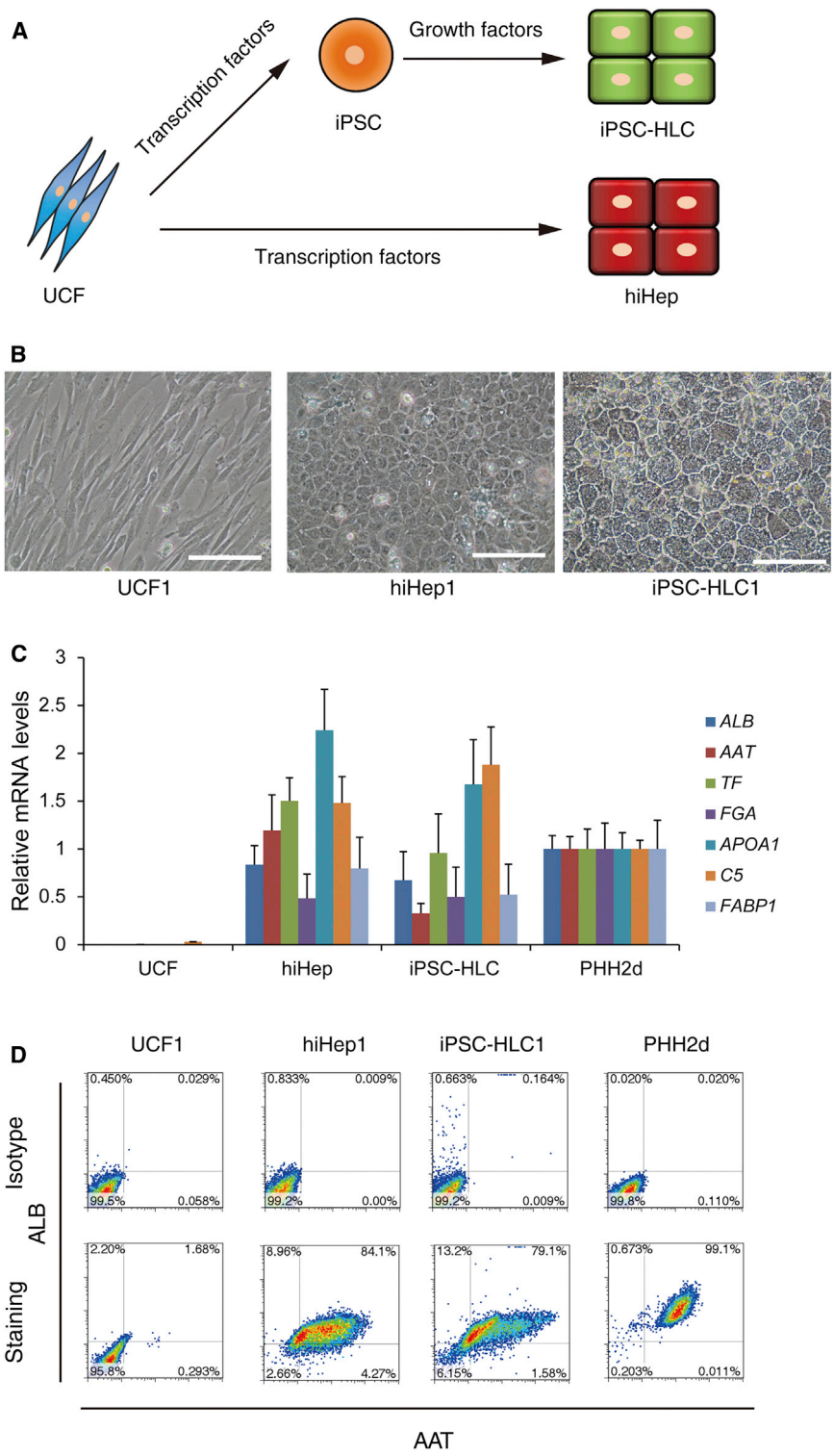

Figure 1. Generation of Hepatocyte-like Cells (HLCs) by Different Strategies

(A) Schematic diagram of the generation of HLCs by different strategies.

(B) Typical morphology of UCF, hiHep, and iPSC-HLC. hiHep1 and iPSC-HLC1 were derived from UCF1. Scale bar, 100 μm.

(C) Hepatic gene expression levels of HLCs were measured by qPCR. UCF included two independent replicates, UCF1 and UCF2; hiHep included four replicates from independent experiments (hiHep1, hiHep2, hiHep3, and hiHep4); iPSC-HLC included four replicates from independent experiments (iPSC-HLC1, iPSC-HLC2, iPSC-HLC3, and iPSC-HLC4); PHH included two independent replicates that were cultured for 2 days.

(D) Both hiHeps and iPSC-HLCs displayed a high percentage of ALB and AAT double-positive cells, as measured by flow cytometry. UCFs were used as negative control and PHHs cultured for 2 days were used as positive control.

See also Figures S1 and S2 and Table S1.

measured testosterone elimination as an indication of CYP3A function in iPSC-HLCs and hiHeps. Both cells could eliminate testosterone to ~20%–30% of the original level within 4 hr (Figure 3C). This was approximately 10- to 15-fold less than PHHs. We next analyzed the biliary excretion capabilities. Both hiHeps and iPSC-HLCs expressed biliary excretion-related transporters (Figure S3D) and showed a high biliary excretion index (BEI), effluxing substrates

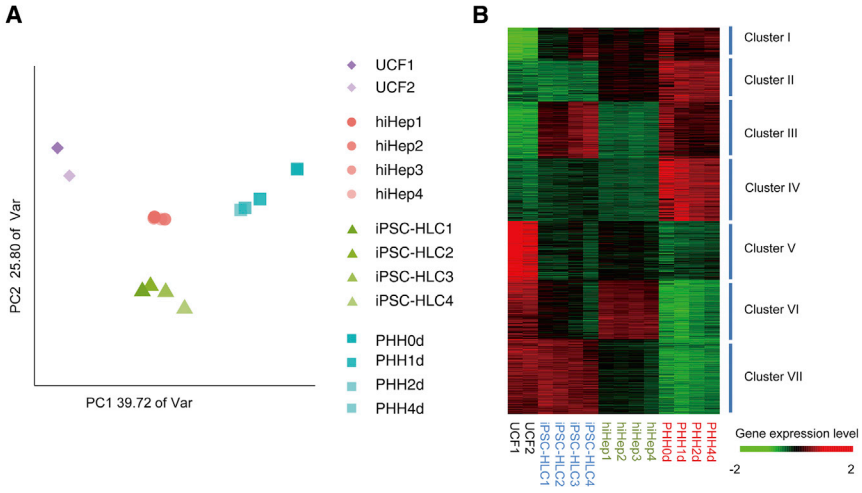

C

Clusters	Enriched Pathways	Representative Genes
Cluster I	Fat digestion and absorption	*APOB*, *APOA1*, *APOM*, *FABP1*, *MTTP*
	Metabolic enzymes	*UGT2A3*, *ACAT2*, *GPX3*, *ACOX1*, *ABCC3*, *TF*
	Complement and coagulation cascades	*FGG*, *FGB*, *CFI*, *AAT*
Cluster II	Cytochrome P450 enzymes	*CYP2A6*, *CYP2B6*, *CYP2A7*, *CYP4A11*
	Phase II metabolic enzymes	*UGT1A1*, *UGT1A6*, *UGT1A7*, *UGT1A9*, *UGT2B15*
	ABC transporters	*ABCC2*, *ABCB1*, *SLC2A9*
	Secreted proteins	*CP*, *FGL1*, *ALB*
	Complement and coagulation cascades	*C4A*, *C4B*, *C2*, *C9*, *ACSL1*
Cluster III	Fat digestion and absorption	*APOA4*, *APOE*, *APOC1*, *APOC2*, *APOA2*
	Complement and coagulation cascades	*F2*, *F7*, *F10*, *FGA*
	Metabolic enzymes	*GSTA1*, *GSTA2*, *CYP1A1*, *CPS1*
	Tight junction	*OCLN*, *TJP3*, *GJB1*, *CDH1*, *CLDN7*
	Bile secretion	*SLCO2B1*, *RXRA*, *SLC22A7*, *SLC51A*, *SLC10A1*
Cluster IV	Cytochrome P450 enzymes	*CYP2C9*, *CYP2E1*, *CYP3A4*, *CYP2C8*, *CYP2C19*
	Phase II metabolic enzymes	*UGT2B7*, *UGT1A4*, *UGT1A3*
	Other Metabolic enzymes	*PON1*, *ARG1*
	Complement and coagulation cascades	*F5*, *F9*, *F11*, *F12*, *C3*, *C6*
	Acute-phase reactants	*ORM1*, *ORM2*, *CRP*

Figure 2. Transcriptome Analysis of hiHeps and iPSC-HLCs

(A) Principal component analysis (PCA) of four cell types using 4,000 genes with highest variance in UCFs and PHHs cultured for 1, 2, and 4 days. The percentages on the axes represent the variance explained by the respective axes. hiHep1 and hiHep2 were derived from UCF1, hiHep3 and hiHep4 were derived from UCF2; iPSC-HLC1 and iPSC-HLC2 were derived from iPSC1, iPSC-HLC3 and iPSC-HLC4 were derived from iPSC2. PHHs were fresh, or cultured for 1, 2, and 4 days.

(B) Hierarchical clustering of UCFs, hiHeps, iPSC-HLCs, and PHHs using 4,000 genes with highest variance in UCFs and PHHs cultured for 1, 2, and 4 days. The samples are the same as (A).

(C) Enriched pathways and representative genes in different cluster groups are summarized.

See also Figure S4 and Table S2.

cholyl-lysyl-fluorescein (CLF), D8-taurocholic acid (D8-TCA), and rosuvastatin at similar levels to PHH (Figure S3E). These results suggested that hiHeps and iPSC-HLCs possessed multiple hepatic functions at comparable levels.

Despite the above similarity between iPSC-HLCs and hiHeps, expression profile analysis predicted that iPSC-HLCs had faster lipid metabolism than hiHeps, whereas hiHeps might perform better in phase II metabolism. Indeed, lipid formation and accumulation in iPSC-HLCs was similar to that in PHHs and almost double than that in hiHeps (Figures 3D and 3E). In accordance with the transcriptomic datasets, we observed that hiHeps possessed greater UGT activity than iPSC-HLCs (Figure 3F).

Understanding iPSC-HLCs and hiHeps Cell Identity *In Vitro*

Next, we asked whether iPSC-HLCs and hiHeps retain molecular traces of their induction processes and whether those molecular traces are important components of hiHep and iPSC-HLC cell identity. We first characterized the elimination of fibroblast-specific gene expression in iPSC-HLCs and hiHeps. Markedly, fibroblast-related genes, selected according to published data (Buganim et al., 2012; Huang et al., 2014), were significantly extinguished in both iPSC-HLCs and hiHeps. Those included *COL1A1*, *COL1A2*, *MMP14*, and *LOXL2* (Figures 4A, S4B, and S4C). However, some fibrotic genes were expressed at low levels in both iPSC-HLCs and hiHep cells (Figure 4A). These data suggest that the original fibroblast identity was efficiently but not fully erased in both hiHeps and iPSC-HLCs.

We next investigated whether iPSC-HLCs and hiHeps retain any molecular traces related to transdifferentiation and differentiation. We first analyzed marker genes of bile duct cells, which share common progenitors with hepatocytes. Expression pattern analysis did not show

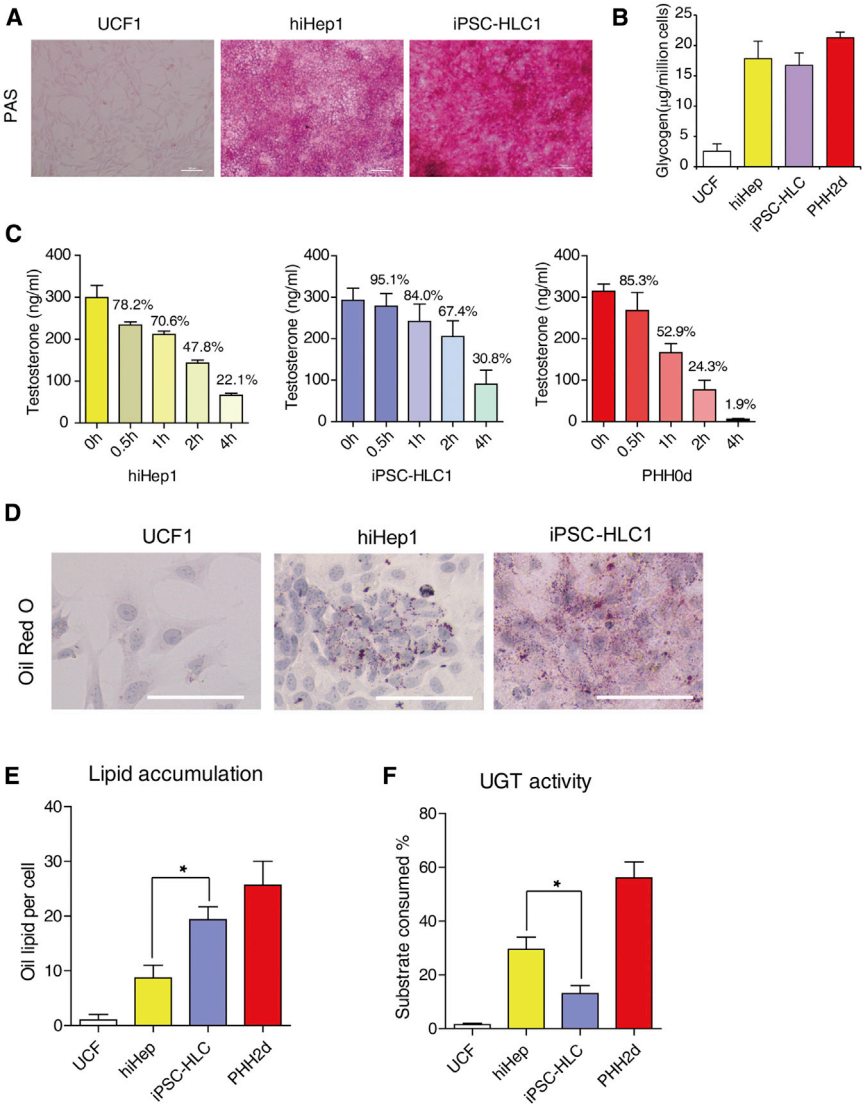

Figure 3. Functional Characterizations of hiHeps and iPSC-HLCs

(A) Glycogen storage in different HLCs was measured by periodic acid-Schiff (PAS) staining. Scale bar, 100 μm.

(B) Glycogen storage in HLCs was determined quantitatively by colorimetric measurement (Abnova). UCF included two independent replicates, UCF1 and UCF2; hiHep included four replicates from independent experiments (hiHep1, hiHep2, hiHep3, and hiHep4); iPSC-HLC included four replicates from independent experiments (iPSC-HLC1, iPSC-HLC2, iPSC-HLC3, and iPSC-HLC4). PHH included two replicates cultured for 2 days from independent experiments.

(C) HLCs both eliminated testosterone as efficiently as PHHs. Concentrations of testosterone were determined by liquid chromatography-tandem mass spectrometry. Each time point had three replicates from independent experiments.

(D) iPSC-HLCs showed more lipid accumulation than hiHep as measured by oil red O staining. Scale bar, 100 μm.

(E) Lipid accumulation was quantified by oil lipid numbers per cell. UCF had two independent replicates, UCF1 and UCF2; hiHep had four replicates from independent experiments (hiHep1, hiHep2, hiHep3, and hiHep4); iPSC-HLC had four replicates from independent experiments (iPSC-HLC1, iPSC-HLC2, iPSC-HLC3, and iPSC-HLC4). PHH included two replicates cultured for 2 days from independent experiments. There was a significant difference between hiHep and iPSC-HLC. *$p < 0.05$.

(F) UGT activities of hiHeps and iPSC-HLCs were determined by the luminescence of remaining substrates. The combination of replicates is the same as in (E). There was a significant difference between hiHep and iPSC-HLC. *$p < 0.05$.

See also Figure S3.

significant bile duct gene expression in both hiHeps and iPSC-HLCs (Figure 4B). Following this, we analyzed for the expression of colon-specific genes (Forster et al., 2014). Notably, the expression of colon-specific genes was undetectable in hiHeps, indicating the specificity of the applied hepatic transdifferentiation protocol (Figure 4C). Interestingly, *CDX2* was detected at low levels in iPSC-HLCs, indicating that low-level colon signatures persist *in vitro* (Figure S5C).

Following these studies, we characterized whether iPSC-HLCs retain molecular traces of endoderm progenitors (Cheng et al., 2012; Loh et al., 2014) and hepatoblasts (Yu et al., 2013). Intriguingly, iPSC-HLCs expressed several marker genes for endoderm progenitors (including *FOXA2* and *GATA6*), and hepatoblasts (including *AFP* and *EPCAM*) (Figures 4D, 4E, and S4D). In contrast, these progenitor marker genes were undetectable in hiHeps, while the iPSC-HLCs expressed less *ALBUMIN* and *TAT* mRNA than the hiHep as shown in RNA-seq analysis (Figure S4D). The expression of progenitor marker genes was validated by q-PCR in iPSC-HLCs (Figure S5A). We performed co-staining for ALB (a marker for mature hepatocytes) and AFP (a marker for immature hepatocytes) in HLCs (Figure S5B). It was striking that almost all iPSC-HLCs were double positive for ALB and AFP, whereas no AFP-positive cells were detectable in hiHeps, suggesting that iPSC-HLCs retained some progenitor traces during the differentiation process.

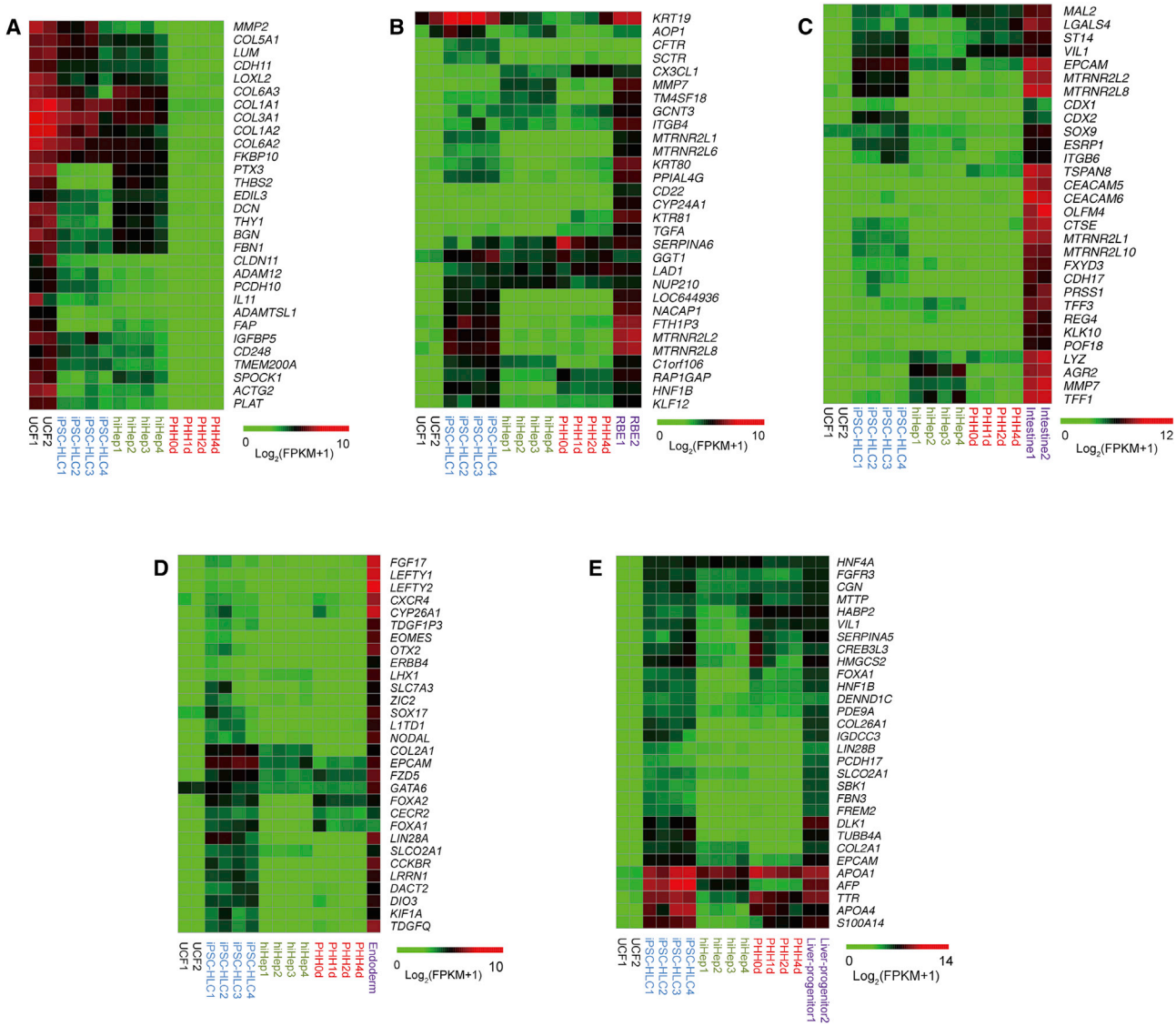

Figure 4. Different Strategies Generate HLCs with Different Gene Expression Patterns

(A) A small amount of fibrotic genes remained after hiHep direct transdifferentiation from fibroblasts. hiHep1 and hiHep2 were derived from UCF1, hiHep3 and hiHep4 were derived from UCF2; iPSC-HLC1 and iPSC-HLC2 were derived from iPSC1, iPSC-HLC3 and iPSC-HLC4 were derived from iPSC2. PHHs were fresh, or cultured for 1, 2, and 4 days.

(B and C) hiHeps did not express cholangiocyte (B) and intestine (C) lineage-specific genes. The combination of replicates is the same as in (A).

(D and E) iPSC-HLCs remained definitive in endoderm (D) and liver progenitor (E) specific gene expression. The combination of replicates is the same as (A).

See also Figures S4 and S5 and Table S2.

Active Histone Modifications Are Detected during hiHeps and iPSC-HLCs

The characteristics of a differentiated cell are stably maintained by histone modifications (Holmberg and Perlmann, 2012). In our experiments, we chose to analyze an active pattern of histone modification, H3K27 acetylation (H3K27ac) at active enhancer and promoter regions in both iPSC-HLCs and hiHeps. Furthermore, UCFs and fresh human adult liver were used as negative and positive controls (Bonn et al., 2012; Creyghton et al., 2010) (Table S2). The genome-wide analysis of H3K27ac occupancy exhibited different patterns between the samples (Figures 5A and S6A) and was divided into eight different clusters. Cluster A included genes that have similar H3K27ac modifications

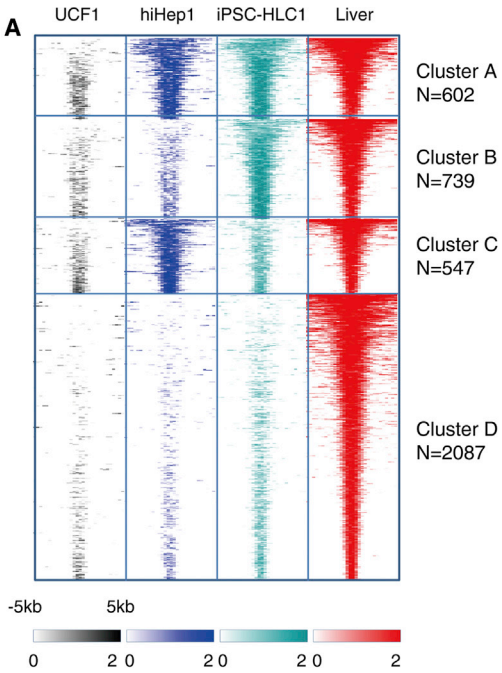

B

Clusters	Representative genes
Cluster A	*ALB*, *APOB*, *ASL*, *CDH1*, *CLDN1*, *FASN*, *FGA*, *FOXO1*, *NR1H3*, *AAT*, *TJP2*
Cluster B	*CYP7B1*,*HNF1B*, *TF*, *KLF15*, *SLC10A1*, *AQP11*, *DNMT3A*, *BMP4*, *FGFR2*
Cluster C	*CYP2C8*, *CYP3A5*, *F5*, *FGB*, *FGL1*, *HHEX*, *PPARG*, *UGT1A1*, *UGT1A9*, *LAMA4*
Cluster D	*ABCB11*, *CYP2C9*, *CYP2E1*, *CYP3A4*, *NR1I3*, *ONECUT1*, *TTR*, *F10*, *F11*, *C6*, *SLCO1B1*

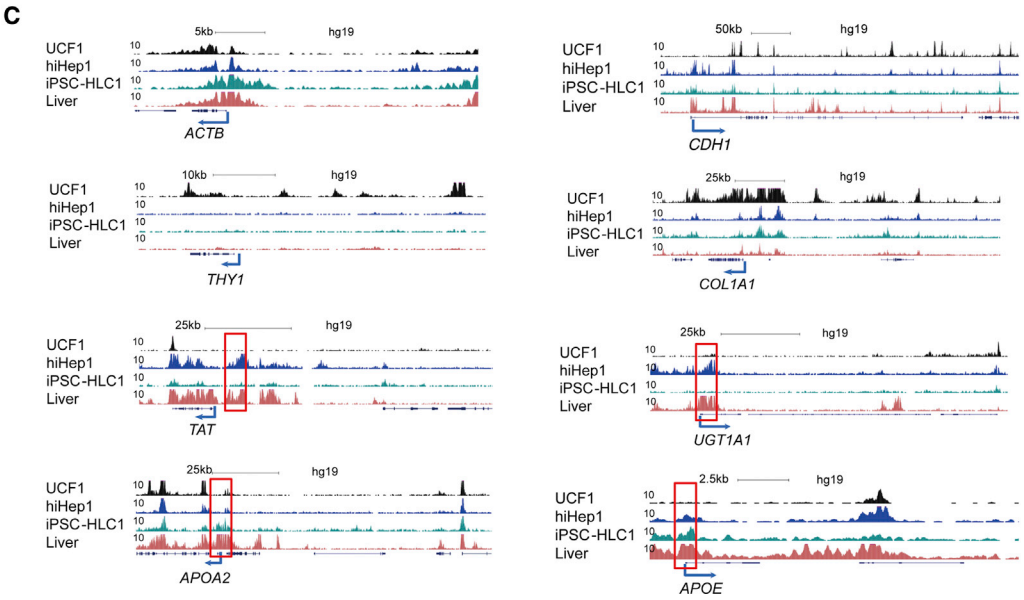

Figure 5. Characterization of H3K27ac Occupancy in Different Cell Types

(A) Distribution of the H3K27ac signals in the four samples. Genes that have H3K27ac in liver but not in UCF1 are shown.

(B) Gene Ontology analysis for the genes associated with H3K27ac peaks in different cluster groups in (A).

(C) Representative tracks of H3K27ac occupancy at housekeeping gene (*ACTB*), fibroblast-specific genes (*THY1* and *COL1A1*), hepatic specific genes (*CDH1*, *TAT*, *UGT1A1*, *APOA2*, *APOE*) across the four cell types. Red boxes mark the different H3K27ac peaks between hiHeps and iPSC-HLCs.

See also Figure S6 and Table S2.

in both HLCs and liver, including *ALB*, *AAT*, *APOB*, and *CDH1* (Figure 5B). In cluster H, most H3K27ac modifications identified on fibrotic genes were erased in HLCs and liver (Figures S6A and S6B). Cluster D indicated hepatic genes that were not fully modified by H3K27ac in HLCs (Figure 5B). Specifically, the enhancers and promoters near

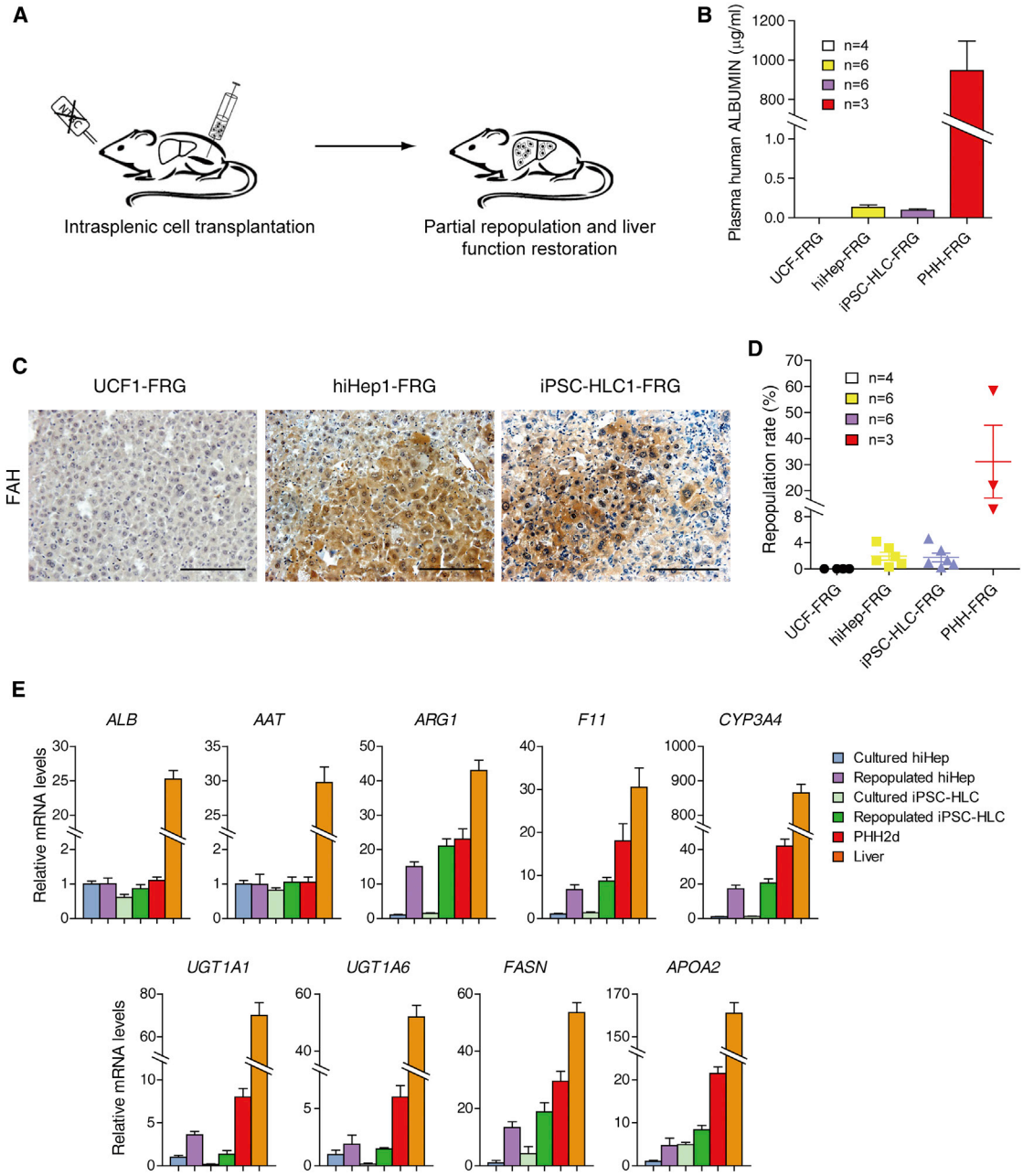

Figure 6. *In Vivo* Characterization and Maturation of hiHeps and iPSC-HLCs after Repopulation

(A) Schematic outline of HLC transplantation into the livers of *Fah*$^{-/-}$/*Rag2*$^{-/-}$/*Il2rg*$^{-/-}$ mice (FRG). Each mouse was transplanted intrasplenically with 5 million HLCs.

(B) Human ALBUMIN levels in the sera of surviving mice from independent experiments were determined by ELISA. UCF-FRG included four mice transplanted with two UCF1 and two UCF2; hiHep-FRG included six mice transplanted with two hiHep1, one hiHep2, two hiHep3, and one hiHep4; iPSC-HLC-FRG included six mice transplanted with two iPSC-HLC1, one iPSC-HLC2, two iPSC-HLC3, and one iPSC-HLC4; PHH-FRG included three mice transplanted with fresh PHHs.

(C) The repopulation of HLCs in FRG mouse livers was determined by immunostaining for FAH. Scale bar, 100 μm.

(D) Repopulation rates of HLCs in the liver of FRG mice were calculated. The combination of replicates is the same as in (B).

(E) FAH-positive hiHeps and iPSC-HLCs were collected by microdissection from serial liver sections. The mRNA levels of indicated genes were measured in repopulated hiHeps and iPSC-HLCs, cultured hiHeps and iPSC-HLCs, PHH and liver by qPCR. Data are normalized to cultured hiHeps. Cultured hiHeps included four replicates from independent experiments (hiHep1, hiHep2, hiHep3. and hiHep4).

(legend continued on next page)

THY1 and *COL1A1* were enriched with H3K27ac in UCFs but erased in hiHeps and iPSC-HLCs (Figure 5C). In contrast, enhancer regions near *CDH1*, *TAT*, *UGT1A1*, *APOA2*, and *APOE* were enriched in H3K27ac in hiHep and iPSC-HLCs when compared with UCFs (Figure 5C). This finding not only demonstrated that both hiHeps and iPSC-HLCs gained stable epigenetic modifications but also proved that hiHeps and iPSC-HLCs had active hepatic gene expression. In accordance with previous analysis, there were differences between iPSC-HLCs and hiHeps with differential acetylation observed at enhancers near *TAT* and *UGT1A1* in hiHep, whereas in iPSC-HLCs, enhancers near *APOA2* and *APOE* were more active (Figure 5C).

Improvements in Hepatocyte Phenotype Were Detected Following hiHep and iPSC-HLC Transplant *In Vivo*

The analysis of histone active markers partially explained the similarities and differences between iPSC-HLCs and hiHeps. Given the plasticity of histone modifications, it is possible to further improve the hepatic features of iPSC-HLCs and hiHeps if a niche is supplied. We decided to transplant these cells into the liver, which may represent the best microenvironment for hepatocytes. hiHeps and iPSC-HLCs were transplanted into *Fah*$^{-/-}$*Rag2*$^{-/-}$*Il2rg*$^{-/-}$ (FRG) mice via splenic injection. FRG mice were kept alive with a supply of 2-(2-nitro-4-trifluoro-methylbenzyol)-1,3-cyclohexanedione (NTBC). After NTBC withdrawal, FRG mice usually die of metabolic liver disease within 4–6 weeks (Azuma et al., 2007). We transplanted five million hiHeps and iPSC-HLCs into FRG mice and analyzed liver repopulation after transplantation (Figure 6A). FRG mice transplanted with UCF and PHH were used as controls. After 2 months, human ALBUMIN levels were at comparable levels in the sera of FRG mice transplanted with hiHeps (153 ± 42 ng/mL) and iPSC-HLCs (114 ± 50 ng/mL) but were low compared with PHHs (0.91 ± 0.16 mg/mL) (Figure 6B). Immunohistochemical staining for human FAH showed that repopulation efficiencies were similar for hiHeps and iPSC-HLCs with contributions ranging from 0.3% to 4.2% (1.95% ± 1.49%) and 0.2%–4.6% (1.75% ± 1.65%) respectively, which were much lower than that of PHHs (Figures 6C, 6D, and S6C). Even though HLCs could repopulate into the livers of FRG mice, they did not secret human ALBUMIN as efficiently as PHHs, which suggested that they were not mature enough for hepatic function.

To evaluate whether hiHeps and iPSC-HLCs were further matured following exposure to the *in vivo* niche, we micro-dissected repopulated nodules from liver sections. Expression of hepatocyte genes was determined in hiHeps and iPSC-HLCs by qPCR using human-specific primers. Compared with cultured hiHeps and iPSC-HLCs, the expression levels of several genes were significantly increased after repopulation, including *CYP3A4* and *F11* (Figure 6E). In addition, we characterized the mRNA levels of lipid metabolism and phase II metabolism-related genes. Markedly, the expression differences discovered in cultured HLCs were normalized in repopulated hiHeps and iPSC-HLCs, suggesting that the *in vivo* microenvironment improved hepatic gene expression. Taken together, our results demonstrate that iPSC-HLCs and hiHeps have the potential to be further matured if the niche they are maintained in is supportive.

DISCUSSION

To rule out donor variability, iPSC-HLCs and hiHeps were generated from the same parental cells (Kajiwara et al., 2012; Ma et al., 2014). In general, both types of HLCs were comparable, with gene expression patterns similar to PHHs, but with obvious differences. *In vitro* functional analysis demonstrated that iPSC-HLCs and hiHeps were comparable, with HLCs demonstrating glycogen storage, ALBUMIN, alpha-1-antitrypsin, and biliary excretion. Notably, when iPSC-HLCs and hiHeps were transplanted into mouse livers, they repopulated the liver at comparable levels and demonstrated comparable gene expression. Taken together, these findings demonstrate that both directed differentiation and transdifferentiation successfully instruct hepatic differentiation, cell engraftment *in vivo*, and similar maturation.

While similarities were observed, differences between hiHeps and iPSC-HLCs existed *in vitro*. Comparison of global gene expression profiles highlighted that iPSC-HLCs express several endoderm progenitor- and hepatoblast-related marker genes as previously reported (Carpentier et al., 2014; Godoy et al., 2015). The induction of iPSC-HLCs was achieved using an affordable and facile three-staged protocol mimicking certain aspects of human hepatocyte development. The *in vitro* differentiation duration is significantly shorter than human development in utero, therefore residual molecular traces left during iPSC-HLC formation could have restricted cell maturation. In addition, the cell niche, and in particular the extracellular matrix, has been shown to be an important driver of HLC

Repopulated hiHeps included two independent replicates from hiHep1-FRG and two independent replicates from hiHep3-FRG. Cultured iPSC-HLCs included four replicates from independent experiments (iPSC-HLC1, iPSC-HLC2, iPSC-HLC3, and iPSC-HLC4). Repopulated iPSC-HLCs included two independent replicates from iPSC-HLC1-FRG and two independent replicates from iPSC-HLC3-FRG.
See also Figure S6.

differentiation, and therefore these areas require further investigation (Cameron et al., 2015).

It was previously reported that mouse iHep cells induced by *Foxa3* and *Hnf4a* express the colon epithelium-specific marker gene *Cdx2*, suggesting that transdifferentiation might detour cells into unwanted lineages if not properly controlled (Morris et al., 2014). However, we did not observe such colon-specific gene expression in our hiHeps. In our studies, the functional assays further validated those findings from gene expression analyses. These data suggest that both iPSC-HLCs and hiHeps have advantages in modeling different aspects of human liver biology "in a dish." Specifically, iPSC-HLCs may be a better model to study fatty liver diseases, whereas hiHeps could be the choice for *in vitro* phase II drug metabolism. HLCs were compared with PHHs with and without culture in this study. While cultured hepatocytes do not completely reflect the nature of primary hepatocytes *in vivo*, they might be sufficient for these types of comparisons if one wishes to normalize the effect caused by *in vitro* culture.

Although functional differences were observed between the HLCs, cell repopulation of immune-deficient $Fah^{-/-}$ mice using iPSC-HLCs or hiHeps was comparable. Importantly, this translated into improvements in liver physiology and murine survival rates providing promise for the clinic in the future. Importantly, iPSC-HLC or hiHep plasticity was observed *in vivo*, indicating that HLCs responded to their environment, leading to improvements in cell phenotype. While these studies demonstrate significant advances, it should be noted that iPSC-HLCs and hiHeps were still not as efficient at engrafting as PHHs in FRG mice. This highlights the need to improve hepatic maturation and/or liver preconditioning, prior to cell transplantation in the future (Fisher and Strom, 2006; Grompe and Strom, 2013; Yang et al., 2017).

Our findings not only suggest potential applications for iPSC-HLCs and hiHeps but also provide insight about the process of differentiation and transdifferentiation. The identification of differentiated cells is mainly determined by regulation of tissue-specific transcription factors and epigenetic modifications (Holmberg and Perlmann, 2012). In support of this, we demonstrate that HLCs generated from both transdifferentiation and directed differentiation had stable epigenetic modifications, which had an impact on their function *in vitro*. These studies also confirm that both hiHeps and iPSC-HLCs are partially differentiated in 2D culture *in vitro*. Going forward, it will be necessary to identify new potential combinations of transcription and growth factors to improve transdifferentiation and directed differentiation. In addition, new strategies such as 3D differentiation (Rashidi et al., 2016; Takebe et al., 2013) and alternative substrates may improve the maturation of both types of HLCs (Cameron et al., 2015; Lim et al., 2016).

Despite the divergences between HLCs and PHHs, HLCs have been already proved useful for *in vitro* disease modeling and cell-based therapies (Forbes et al., 2015; Shi et al., 2016). Going forward, it is critical to unveil the differences that exist between HLCs and PHHs to improve cell phenotype further. This will lead to improved models for the lab and cells for the clinic in the future (Nicolas et al., 2017).

EXPERIMENTAL PROCEDURES

Cell Culture and Generation of Hepatocyte-like Cells

UCFs were cultured in human fibroblast medium. hiHeps were generated from immortalized UCFs with transduction of *FOXA3*, *HNF1A*, and *HNF4A*, and cultured in hepatocyte-maintaining medium as previously reported (Huang et al., 2014). Human iPSCs were generated from UCFs by transduction of retrovirus (*OCT4*, *SOX2*, *KLF4*, and *C-MYC*). iPSC-HLCs were generated from iPSCs through a three-step method as previously reported (Szkolnicka et al., 2014).

Primary Hepatocyte Culture

PHHs from three individuals were purchased from Celsis In Vitro Technologies. PHHs were pooled together in the same number and plated at a density of $1.25 \times 10^5/cm^2$. For the testosterone clearance assay, we used freshly thawed PHHs. For the other assays, the days of culture of PHHs are indicated. Institutional ethical committees approved the collection and use of human samples.

Mice

FRG mice were maintained with NTBC water at a concentration of 16 mg/L. NTBC water was withdrawn 1 week before the transplantation of HLCs. hiHeps and iPSC-HLCs (5×10^6 cells/animal) were injected into the spleens of the mice. All mouse experiments were approved by the Institutional Animal Care and Use Committee of the Institute of Biochemistry and Cell Biology and performed in accordance with institutional guidelines.

RNA-Seq Analysis

Total RNA was isolated from UCFs, hiHeps, iPSC-HLCs, and PHHs by Trizol. RNA-seq libraries were prepared with the Illumina TruSeq RNA Sample Preparation Kit. The fragmented and randomly primed 100 bp paired-end libraries were sequenced on an Illumina HiSeq 2000 sequencing system.

ChIP-Seq Analysis

Chromatin immunoprecipitation (ChIP) was performed using antibodies for acetylation of histone H3 lysine 27 acetylation (H3K27ac, Abcam Ab4729). DNA libraries of matched input and ChIP samples were prepared using the Illumina Truseq kit, indexed for multiplexed runs of four libraries per lane, and sequenced on an Illumina HiSeq2000 instrument.

Statistical Analysis

Data were subjected to Student's t test. $p < 0.05$ was considered statistically significant. Data are presented as means ± SD.

ACCESSION NUMBERS

Original data are available in the NCBI Gene Expression Omnibus under accession number GEO: GSE103078.

SUPPLEMENTAL INFORMATION

Supplemental Information includes Supplemental Experimental Procedures, six figures, and two tables and can be found with this article online at https://doi.org/10.1016/j.stemcr.2017.10.019.

AUTHOR CONTRIBUTIONS

L.H. and G.W. conceived and supervised the study. Y.G. performed most of the experiments. X.Z. analyzed the RNA-seq and ChIP-seq data. L.Z. and J.C. performed the *in vivo* characterization of hiHeps and iPSC-HLCs. X.N., X.L., and G.P. characterized and analyzed the CYP metabolism and drug toxicity. Y.L. performed the H3K27ac ChIP experiment. D.C.H. assisted in the generation and characterization of iPSC-HLCs and manuscript writing. D.L., C.Y., Z.Z., Y.S., X. Chen, and X.Cheng helped with the preparation of UCF and characterization of human iPSCs. Y.G., X.Z., G.W., and L.H. analyzed the data and wrote the paper with suggestions from the other authors.

ACKNOWLEDGMENTS

We are thankful to Dr. Yunwen Zheng (University of Tsukuba, Japan) for his suggestions on the experiments. This study is supported by CAS- CSIRO (153D31KYSB20160247), CAS-NWO Programme (153D31KYSB20150085), the National Natural Science Foundation of China (NSFC; 31630044, 31601186, 81471948, 31771431, 31271354, and 31401263), the Ministry of Science and Technology of China (MOST; 2013CB967103), the Science and Technology Commission of Shanghai Municipality (STCSM; 16JC1400202 and 15JC1400200), and Shanghai Zhangjiang National Independent Innovation Demonstration Zone Stem Cells Translational Medicine Industry Base Project (ZJ2014-ZD-002). D.C.H. was supported by the UK Regenerative Medicine Platform award (MR/L022974/1).

Received: July 24, 2017
Revised: October 22, 2017
Accepted: October 23, 2017
Published: November 22, 2017

REFERENCES

Azuma, H., Paulk, N., Ranade, A., Dorrell, C., Al-Dhalimy, M., Ellis, E., Strom, S., Kay, M.A., Finegold, M., and Grompe, M. (2007). Robust expansion of human hepatocytes in Fah-/-/Rag2-/-/Il2rg-/- mice. Nat. Biotechnol. *25*, 903–910.

Bhatia, S.N., Underhill, G.H., Zaret, K.S., and Fox, I.J. (2014). Cell and tissue engineering for liver disease. Sci. Transl. Med. *6*, 245sr2.

Bonn, S., Zinzen, R.P., Girardot, C., Gustafson, E.H., Perez-Gonzalez, A., Delhomme, N., Ghavi-Helm, Y., Wilczynski, B., Riddell, A., and Furlong, E.E. (2012). Tissue-specific analysis of chromatin state identifies temporal signatures of enhancer activity during embryonic development. Nat. Genet. *44*, 148–156.

Buganim, Y., Itskovich, E., Hu, Y.C., Cheng, A.W., Ganz, K., Sarkar, S., Fu, D.D., Welstead, G.G., Page, D.C., and Jaenisch, R. (2012). Direct reprogramming of fibroblasts into embryonic Sertoli-like cells by defined factors. Cell Stem Cell *11*, 373–386.

Cameron, K., Tan, R., Schmidt-Heck, W., Campos, G., Lyall, M.J., Wang, Y., Lucendo-Villarin, B., Szkolnicka, D., Bates, N., Kimber, S.J., et al. (2015). Recombinant laminins drive the differentiation and self-organization of hESC-derived hepatocytes. Stem Cell Reports *5*, 1250–1262.

Carpentier, A., Tesfaye, A., Chu, V., Nimgaonkar, I., Zhang, F., Lee, S.B., Thorgeirsson, S.S., Feinstone, S.M., and Liang, T.J. (2014). Engrafted human stem cell-derived hepatocytes establish an infectious HCV murine model. J. Clin. Invest. *124*, 4953–4964.

Cheng, X., Ying, L., Lu, L., Galvao, A.M., Mills, J.A., Lin, H.C., Kotton, D.N., Shen, S.S., Nostro, M.C., Choi, J.K., et al. (2012). Self-renewing endodermal progenitor lines generated from human pluripotent stem cells. Cell Stem Cell *10*, 371–384.

Creyghton, M.P., Cheng, A.W., Welstead, G.G., Kooistra, T., Carey, B.W., Steine, E.J., Hanna, J., Lodato, M.A., Frampton, G.M., Sharp, P.A., et al. (2010). Histone H3K27ac separates active from poised enhancers and predicts developmental state. Proc. Natl. Acad. Sci. USA *107*, 21931–21936.

Du, Y., Wang, J., Jia, J., Song, N., Xiang, C., Xu, J., Hou, Z., Su, X., Liu, B., Jiang, T., et al. (2014). Human hepatocytes with drug metabolic function induced from fibroblasts by lineage reprogramming. Cell Stem Cell *14*, 394–403.

Fisher, R.A., and Strom, S.C. (2006). Human hepatocyte transplantation: worldwide results. Transplantation *82*, 441–449.

Forbes, S.J., Gupta, S., and Dhawan, A. (2015). Cell therapy for liver disease: from liver transplantation to cell factory. J. Hepatol. *62*, S157–S169.

Forster, R., Chiba, K., Schaeffer, L., Regalado, S.G., Lai, C.S., Gao, Q., Kiani, S., Farin, H.F., Clevers, H., Cost, G.J., et al. (2014). Human intestinal tissue with adult stem cell properties derived from pluripotent stem cells. Stem Cell Reports *2*, 838–852.

Fox, I.J., Daley, G.Q., Goldman, S.A., Huard, J., Kamp, T.J., and Trucco, M. (2014). Stem cell therapy. Use of differentiated pluripotent stem cells as replacement therapy for treating disease. Science *345*, 1247391.

Gerbal-Chaloin, S., Funakoshi, N., Caillaud, A., Gondeau, C., Champon, B., and Si-Tayeb, K. (2014). Human induced pluripotent stem cells in hepatology: beyond the proof of concept. Am. J. Pathol. *184*, 332–347.

Godoy, P., Schmidt-Heck, W., Natarajan, K., Lucendo-Villarin, B., Szkolnicka, D., Asplund, A., Bjorquist, P., Widera, A., Stober, R., Campos, G., et al. (2015). Gene networks and transcription factor motifs defining the differentiation of stem cells into hepatocyte-like cells. J. Hepatol. *63*, 934–942.

Grompe, M., and Strom, S. (2013). Mice with human livers. Gastroenterology *145*, 1209–1214.

Hay, D.C., Fletcher, J., Payne, C., Terrace, J.D., Gallagher, R.C., Snoeys, J., Black, J.R., Wojtacha, D., Samuel, K., Hannoun, Z., et al. (2008). Highly efficient differentiation of hESCs to functional hepatic endoderm requires ActivinA and Wnt3a signaling. Proc. Natl. Acad. Sci. USA *105*, 12301–12306.

Holmberg, J., and Perlmann, T. (2012). Maintaining differentiated cellular identity. Nat. Rev. Genet. *13*, 429–439.

Huang, P., Zhang, L., Gao, Y., He, Z., Yao, D., Wu, Z., Cen, J., Chen, X., Liu, C., Hu, Y., et al. (2014). Direct reprogramming of human fibroblasts to functional and expandable hepatocytes. Cell Stem Cell *14*, 370–384.

Kajiwara, M., Aoi, T., Okita, K., Takahashi, R., Inoue, H., Takayama, N., Endo, H., Eto, K., Toguchida, J., Uemoto, S., et al. (2012). Donor-dependent variations in hepatic differentiation from human-induced pluripotent stem cells. Proc. Natl. Acad. Sci. USA *109*, 12538–12543.

Lim, K.T., Lee, S.C., Gao, Y., Kim, K.P., Song, G., An, S.Y., Adachi, K., Jang, Y.J., Kim, J., Oh, K.J., et al. (2016). Small molecules facilitate single factor-mediated hepatic reprogramming. Cell Rep. *15*, 814–829.

Loh, K.M., Ang, L.T., Zhang, J., Kumar, V., Ang, J., Auyeong, J.Q., Lee, K.L., Choo, S.H., Lim, C.Y., Nichane, M., et al. (2014). Efficient endoderm induction from human pluripotent stem cells by logically directing signals controlling lineage bifurcations. Cell Stem Cell *14*, 237–252.

Ma, H., Morey, R., O'Neil, R.C., He, Y., Daughtry, B., Schultz, M.D., Hariharan, M., Nery, J.R., Castanon, R., Sabatini, K., et al. (2014). Abnormalities in human pluripotent cells due to reprogramming mechanisms. Nature *511*, 177–183.

Morris, S.A., Cahan, P., Li, H., Zhao, A.M., San Roman, A.K., Shivdasani, R.A., Collins, J.J., and Daley, G.Q. (2014). Dissecting engineered cell types and enhancing cell fate conversion via CellNet. Cell *158*, 889–902.

Nicolas, C.T., Hickey, R.D., Chen, H.S., Mao, S.A., Lopera Higuita, M., Wang, Y., and Nyberg, S.L. (2017). Concise review: liver regenerative medicine: from hepatocyte transplantation to bioartificial livers and bioengineered grafts. Stem Cells *35*, 42–50.

Rashidi, H., Alhaque, S., Szkolnicka, D., Flint, O., and Hay, D.C. (2016). Fluid shear stress modulation of hepatocyte-like cell function. Arch. Toxicol. *90*, 1757–1761.

Rezvani, M., Grimm, A.A., and Willenbring, H. (2016). Assessing the therapeutic potential of lab-made hepatocytes. Hepatology *64*, 287–294.

Shi, X.L., Gao, Y., Yan, Y., Ma, H., Sun, L., Huang, P., Ni, X., Zhang, L., Zhao, X., Ren, H., et al. (2016). Improved survival of porcine acute liver failure by a bioartificial liver device implanted with induced human functional hepatocytes. Cell Res. *26*, 206–216.

Si-Tayeb, K., Noto, F.K., Nagaoka, M., Li, J., Battle, M.A., Duris, C., North, P.E., Dalton, S., and Duncan, S.A. (2010). Highly efficient generation of human hepatocyte-like cells from induced pluripotent stem cells. Hepatology *51*, 297–305.

Sullivan, G.J., Hay, D.C., Park, I.H., Fletcher, J., Hannoun, Z., Payne, C.M., Dalgetty, D., Black, J.R., Ross, J.A., Samuel, K., et al. (2010). Generation of functional human hepatic endoderm from human induced pluripotent stem cells. Hepatology *51*, 329–335.

Szkolnicka, D., Farnworth, S.L., Lucendo-Villarin, B., and Hay, D.C. (2014). Deriving functional hepatocytes from pluripotent stem cells. Curr. Protoc. Stem Cell Biol. *30*, 1G.5.1–1G.5.12.

Szkolnicka, D., and Hay, D.C. (2016). Concise review: advances in generating hepatocytes from pluripotent stem cells for translational medicine. Stem Cells *34*, 1421–1426.

Takahashi, K., Tanabe, K., Ohnuki, M., Narita, M., Ichisaka, T., Tomoda, K., and Yamanaka, S. (2007). Induction of pluripotent stem cells from adult human fibroblasts by defined factors. Cell *131*, 861–872.

Takebe, T., Sekine, K., Enomura, M., Koike, H., Kimura, M., Ogaeri, T., Zhang, R.R., Ueno, Y., Zheng, Y.W., Koike, N., et al. (2013). Vascularized and functional human liver from an iPSC-derived organ bud transplant. Nature *499*, 481–484.

Touboul, T., Hannan, N.R., Corbineau, S., Martinez, A., Martinet, C., Branchereau, S., Mainot, S., Strick-Marchand, H., Pedersen, R., Di Santo, J., et al. (2010). Generation of functional hepatocytes from human embryonic stem cells under chemically defined conditions that recapitulate liver development. Hepatology *51*, 1754–1765.

Yang, J., Wang, Y., Zhou, T., Wong, L.Y., Tian, X.Y., Hong, X., Lai, W.H., Au, K.W., Wei, R., Liu, Y., et al. (2017). Generation of human liver chimeric mice with hepatocytes from familial hypercholesterolemia induced pluripotent stem cells. Stem Cell Reports *8*, 605–618.

Yu, B., He, Z.Y., You, P., Han, Q.W., Xiang, D., Chen, F., Wang, M.J., Liu, C.C., Lin, X.W., Borjigin, U., et al. (2013). Reprogramming fibroblasts into bipotential hepatic stem cells by defined factors. Cell Stem Cell *13*, 328–340.

Stem Cell Reports, Volume *9*

Supplemental Information

Distinct Gene Expression and Epigenetic Signatures in Hepatocyte-like Cells Produced by Different Strategies from the Same Donor

Yimeng Gao, Xiaoran Zhang, Ludi Zhang, Jin Cen, Xuan Ni, Xiaoying Liao, Chenxi Yang, Ying Li, Xiaotao Chen, Zhao Zhang, Yajing Shu, Xin Cheng, David C. Hay, Dongmei Lai, Guoyu Pan, Gang Wei, and Lijian Hui

Supplemental Information

Figure S1:

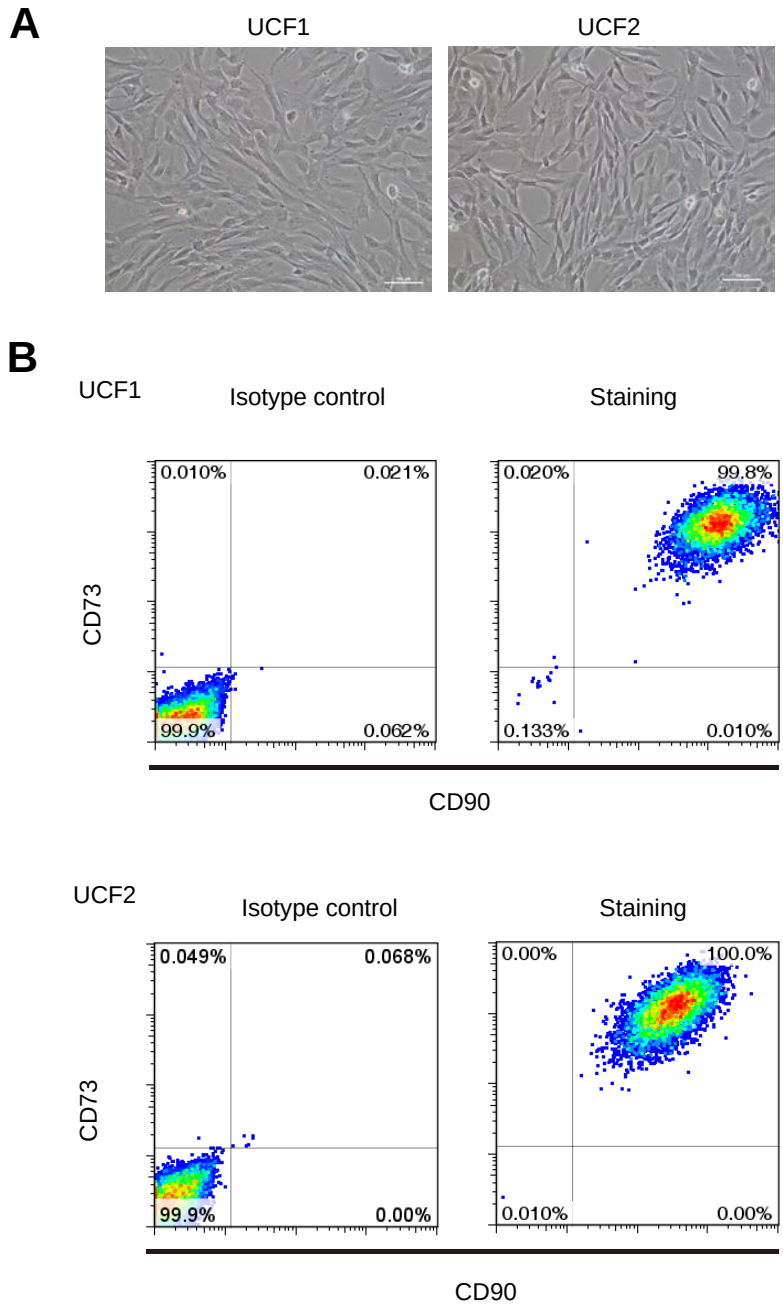

Figure S1. Characterization of umbilical cord-derived fibroblasts (UCF). Related to Figure 1.

(A) Fibroblast-like morphology of two UCFs. Scale bar, 100 μm.

(B) Flow cytometric analysis of surface marker expression on UCFs. Both UCF1 and UCF2 were positive for CD73 and CD90 as measured by flow cytometry.

Figure S2:

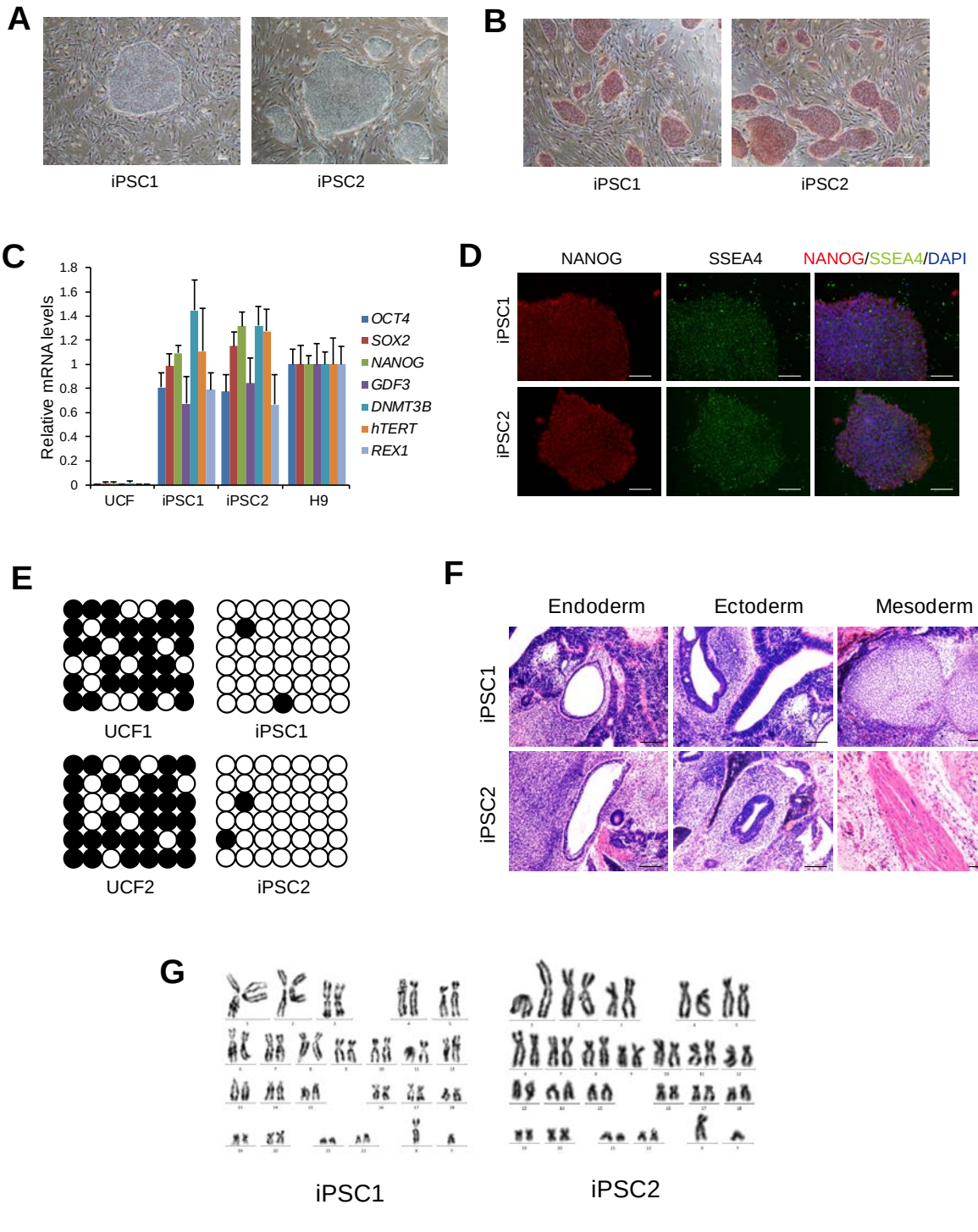
A
iPSC1
iPSC2
B
iPSC1
iPSC2
C
Relative mRNA levels
1.8
1.6
1.4
1.2
1
0.8
0.6
0.4
0.2
0
UCF
iPSC1
iPSC2
H9
OCT4
SOX2
NANOG
GDF3
DNMT3B
hTERT
REX1
D
NANOG
SSEA4
NANOG/SSEA4/DAPI
iPSC1
iPSC2
E
UCF1
iPSC1
UCF2
iPSC2
F
Endoderm
Ectoderm
Mesoderm
iPSC1
iPSC2
G
iPSC1
iPSC2

Figure S2. Characterization of human iPSCs. Related to Figure 1.

(A) iPSC lines showed typical morphology of human embryonic stem cells (ESC). Scale bar, 100 μm.

(B) iPSC lines showed alkaline phosphatase activities as measured by AP staining. Scale bar, 100 μm.

(C) iPSCs showed similar gene expression levels of pluripotent stem cell genes compared with human ESCs (H9).

(D) iPSCs were measured by immunofluorescent staining for pluripotent stem cell specific markers, NANOG and SSEA4. Scale bar, 100 μm.

(E) Bisulfite genomic sequencing of the promoter regions of OCT4. Open and closed circles indicated unmethylated and methylated CpGs.

(F) Hematoxylin and eosin (HE) staining of teratoma derived from iPSC lines. Scale bar, 100 μm.

(G) iPSC lines showed normal karyotypes after long-term culture.

Figure S3:

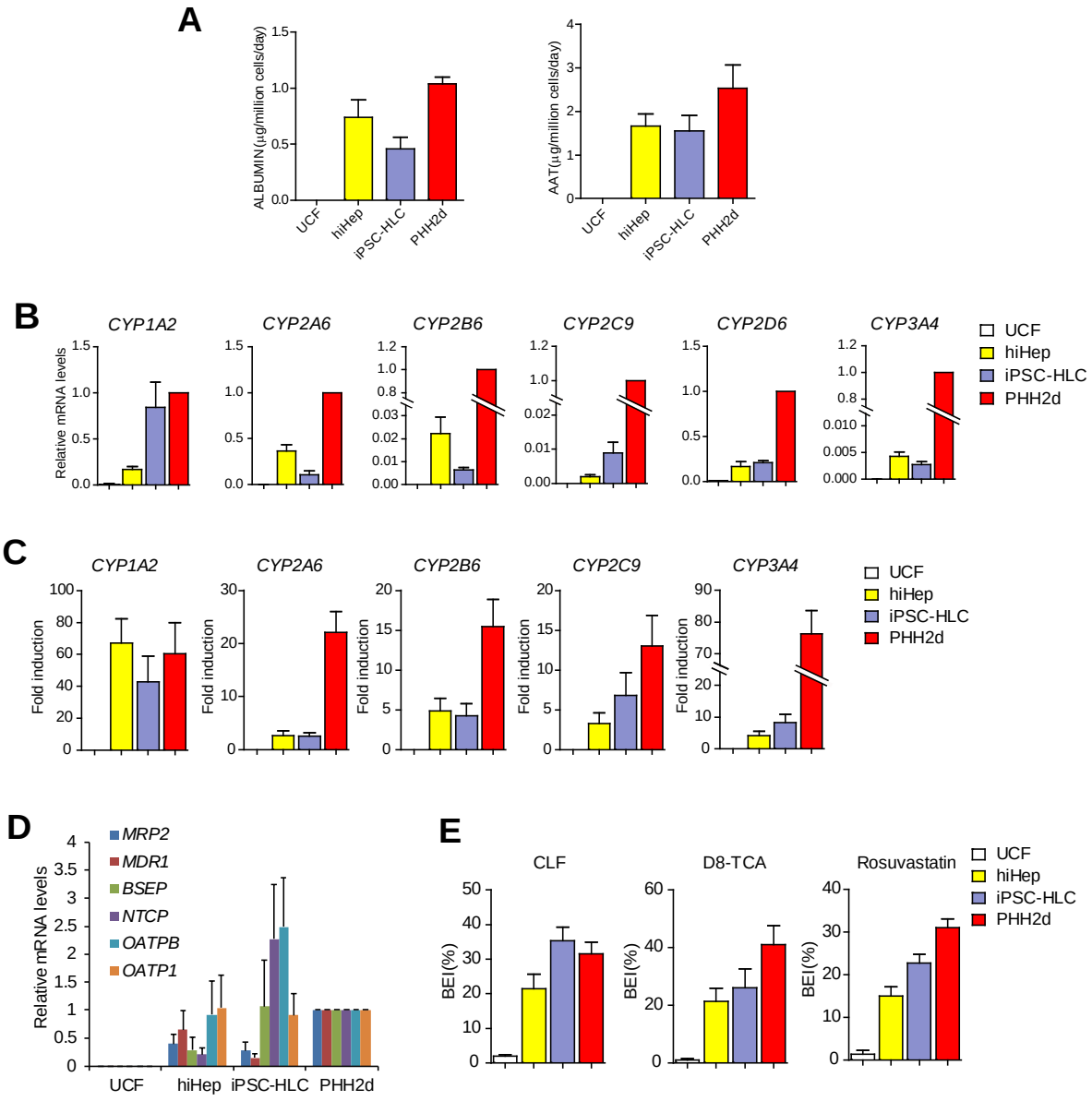
A
ALBUMIN (µg/million cells/day)
AAT (µg/million cells/day)
UCF
hiHep
iPSC-HLC
PHH2d
B
CYP1A2
CYP2A6
CYP2B6
CYP2C9
CYP2D6
CYP3A4
Relative mRNA levels
C
Fold induction
D
MRP2
MDR1
BSEP
NTCP
OATPB
OATP1
Relative mRNA levels
E
CLF
D8-TCA
Rosuvastatin
BEI (%)

Figure S3. *In vitro* characterization of hiHep and iPSC-HLC. Related to Figure 3.

(A) ALBUMIN and α-1-antitrypsin secretion levels were determined by ELISA. UCF included one UCF1 and one UCF2; hiHep included four independent replicates (hiHep1, hiHep2, hiHep3 and hiHep4); iPSC-HLC included four replicates (iPSC-HLC1, iPSC-HLC2, iPSC-HLC3 and iPSC-HLC4); PHHs included two independent replicates which were cultured for two days.

(B) The mRNA levels of Cytochrome P450 (CYP) genes of hiHep and iPSC-HLC were determined by q-PCR. The combination of replicates is the same as Figure S3A.

(C) CYP1A2 can be significantly induced in HLCs, while other CYP genes can be induced slightly. Fold changes were determined by q-PCR. The combination of replicates is the same as Figure S3A.

(D) Transporter expression levels in hiHep and iPSC-HLC were determined by q-PCR. The combination of replicates is the same as Figure S3A.

(E) Biliary excretion capabilities of HLCs were measured by clearance of cholyl-lysyl-fluorescein (CLF), D8-taurocholic acid (D8-TCA) and Rosuvastatin. The combination of replicates is the same as Figure S3A.

Figure S4:

A

Clusters	Enriched Pathways	Representative genes
Cluster V	Regulation of actin cytoskeleton	*FGF7*, *LIMK1*, *PIK3CD*, *TWIST2*, *ITGA11*, *ITGB5*, *MYL9*, *VIM*
	Focal adhesion	*ITGA11*, *ITGB1*, *FLNA*, *VEGFC*, *LAMA4*, *CCND1*, *COL8A1*, *SNAI2*
	Cytokine-cytokine receptor interaction	*CSF3*, *IL6*, *CCL2*, *CXCL8*, *HGF*, *CCL7*, *IL11*, *LIF*, *CXCL1*, *CXCL3*
	Cell adhesion molecules (CAMs)	*NCAM2*, *CD274*, *CNTN1*, *CLDN11*, *ITGA4*, *CDH2*, *JAM2*, *CDH4*
Cluster VI	ECM-receptor interaction	*COL4A2*, *COL4A1*, *ITGB8*, *COL6A3*, *ITGA1*, *TIMP2*, *LOXL2*, *PTX3*
	Focal adhesion	*FLT1*, *ITGA1*, *ITGA3*, *COL5A2*, *LAMA2*, *DOCK1*, *FYN*, *SERPINE2*
	Protein digestion and absorption	*SLC1A5*, *COL7A1*, *COL6A3*, *COL15A1*, *MME*, *COL11A1*, *COL5A2*
	PI3K-Akt signaling pathway	*FGF5*, *ITGB8*, *PDGFRA*, *PDGFRB*, *GNB4*, *COL11A1*, *AKT3*
Cluster VII	ECM-receptor interaction	*LAMA1*, *COL6A2*, *COL1A2*, *COL6A1*, *COL1A1*, *MMP2*, *MMP14*
	Focal adhesion	*SRC*, *LAMB2*, *EGF*, *FN1*, *FLNC*, *COL5A1*, *COL4A6*, *KDR*
	Hippo signaling pathway	*WNT5A*, *BMP4*, *FZD8*, *TEAD2*, *TEAD3*, *WTIP*, *TGFB1*, *BMP6*

B

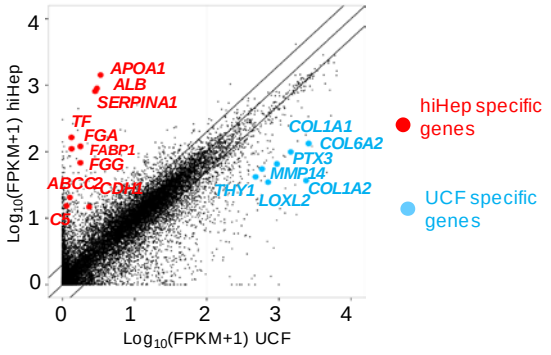

C

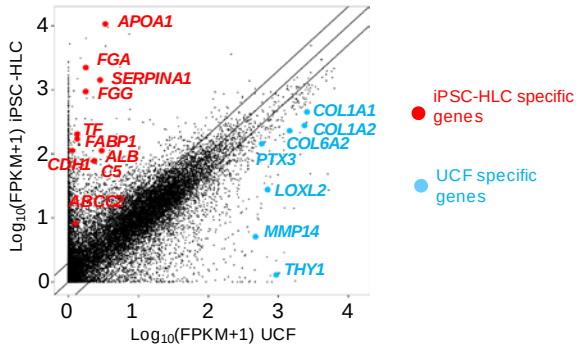

D

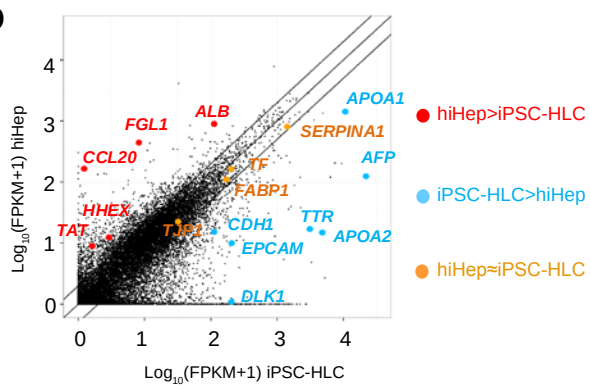

Figure S4. Gene expression analysis of hiHeps and iPSC-HLCs. Related to Figure 2 and Figure 4.

(A) Enriched pathways and representative genes highly expressed in UCFs were summarized.

(B-C) Pair-wise gene expression comparisons showed that most hepatic markers were increased, whereas fibroblast-specific genes were silenced in hiHeps (B) and iPSC-HLCs (C). The combination of replicates is the same as Figure 4A.

(D) A number of hepatic genes expressed differently between hiHeps and iPSC-HLCs. Black lines indicate 2-fold changes between the sample pairs. The combination of replicates is the same as Figure 4A.

Figure S5:

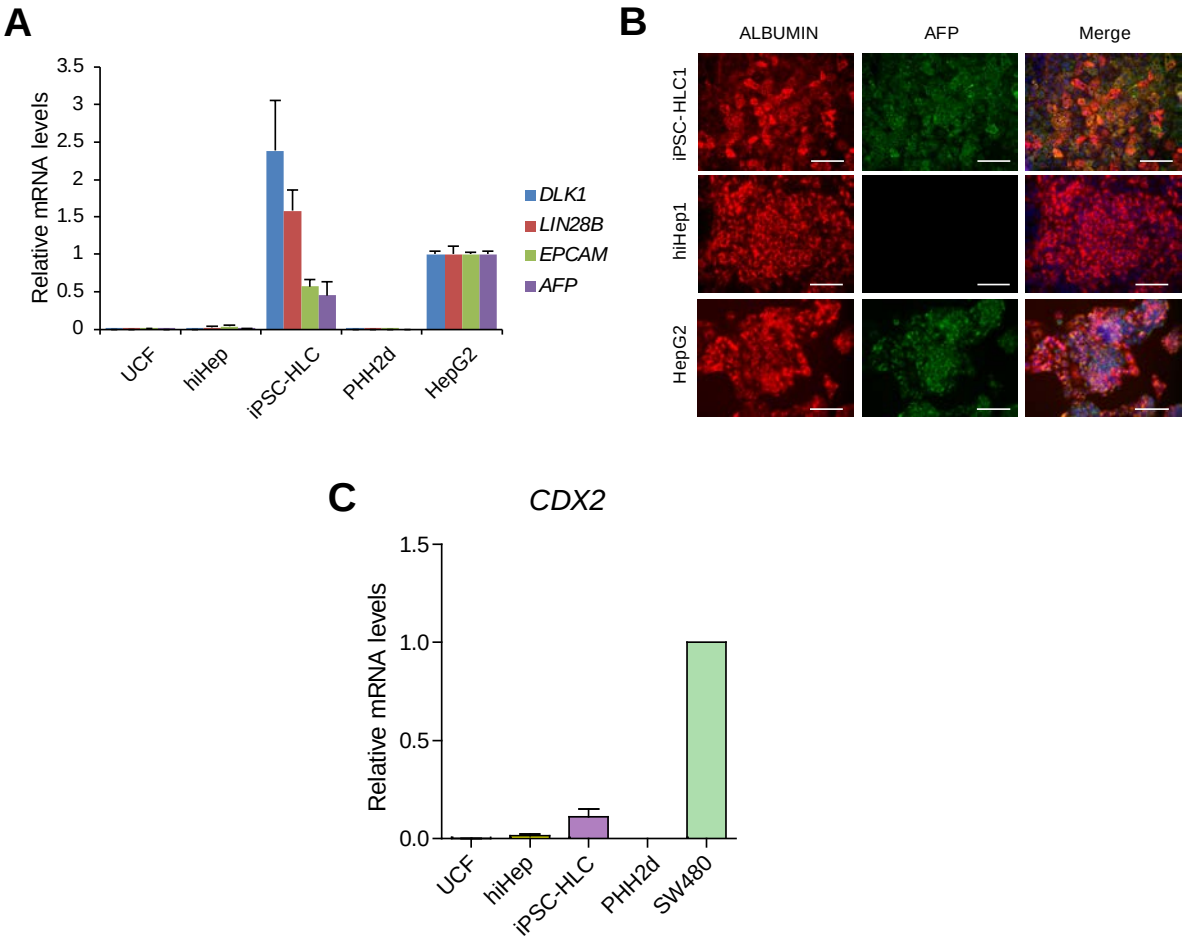
A
Relative mRNA levels
3.5
3
2.5
2
1.5
1
0.5
0
UCF
hiHep
iPSC-HLC
PHH2d
HepG2
DLK1
LIN28B
EPCAM
AFP
B
ALBUMIN
AFP
Merge
iPSC-HLC1
hiHep1
HepG2
C
CDX2
Relative mRNA levels
1.5
1.0
0.5
0.0
UCF
hiHep
iPSC-HLC
PHH2d
SW480

Figure S5. iPSC-HLC expressed immature markers. Related to Figure 4.

(A) Marker genes of immature hepatocytes were expressed in iPSC-HLC, as determined by q-PCR. HepG2 was used as positive control. UCFs included one UCF1 and one UCF2; hiHeps included four independent replicates (hiHep1, hiHep2, hiHep3 and hiHep4); iPSC-HLCs included four independent replicates (iPSC-HLC1, iPSC-HLC2, iPSC-HLC3 and iPSC-HLC4); HepG2 included two replicates.

(B) ALBUMIN and α-fetoprotein (AFP) were co-expressed in iPSC-HLCs, while hiHep expressed ALBUMIN uniquely. HepG2 was used as positive control. Scale bar, 100 μm.

(C) iPSC-HLC showed low CDX2 gene expression level. SW480 was used as positive control. The combination of replicates is the same as Figure S5A.

Figure S6

A

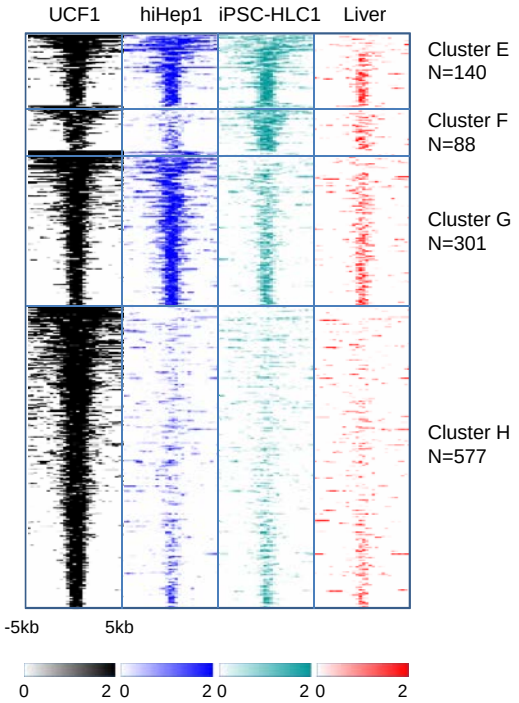

B

Clusters	Representative genes
Cluster E	*CDH11*, *COL5A2*, *IGF2BP1*, *PRC1*, *SLC7A5*
Cluster F	*ALPK2*, *E2F4*, *RARB*, *VCAN*
Cluster G	*CXCL1*, *FOXL1*, *IL8*, *MED24*
Cluster H	*ABCC1*, *COL6A1*, *COL7A1*, *E2F1*, *FGF2*, *IL6*, *MMP2*, *SLC2A6*, *TWIST2*

C

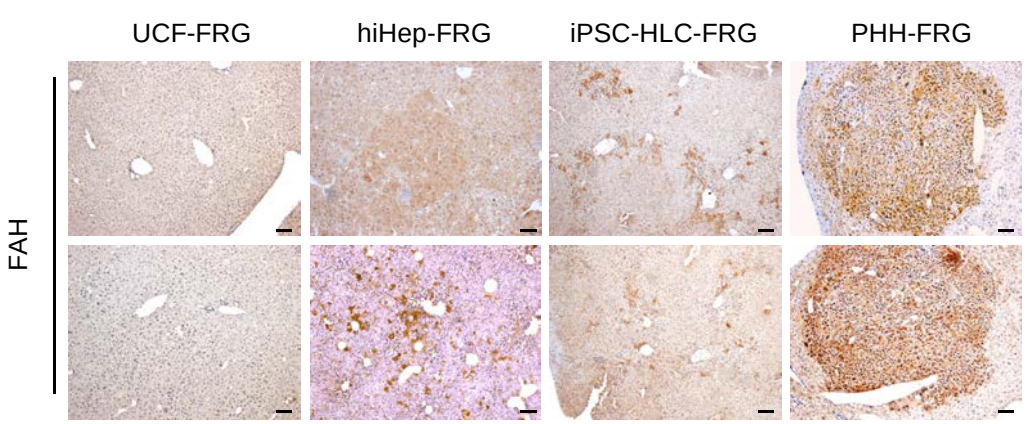

Figure S6. HLCs erased their fibrotic H3K27ac modifications and repopulated in the liver of FRG mice. Related to Figure 5 and Figure 6.

(A) Distribution of the H3K27ac signals in the four samples. Genes which have H3K27ac in UCF1 but not in liver are shown. Each row represents a promoter region of ± 5 kb around the TSS and ranked by the H3K27ac read counts in promoter regions. Peaks were grouped based on presence/absence of peaks comparing the UCF1 and HLCs samples.

(B) Gene Ontology analysis for the genes associated with H3K27ac peaks in different cluster groups.

(C) Representative photos of low magnification showed the engraftment efficiency of HLCs in the livers of FRG mice. Scale bar, 100 μm.

Table S1:

Sample	Donor1			Donor2		
	UCF1	**iPSC-HLC1**	**hiHep1**	**UCF2**	**iPSC-HLC3**	**hiHep3**
SEX	Male	Male	Male	Female	Female	Female
AME	XY	XY	XY	XX	XX	XX
CSF1PO	10,12	10,12	10,12	10,12	10,12	10,12
D5S818	10	10	10	11,12	11,12	11,12
D7S820	10,11	10,11	10,11	10,12	10,12	10,12
D13S317	8,10	8,10	8,10	8	8	8
D16S539	9,11	9,11	9,11	9	9	9
TH01	9,10	9,10	9,10	9	9	9
TPOX	8,9	8,9	8,9	8,10	8,10	8,10
vWA	16,17	16,17	16,17	13,14	13,14	13,14

Table S1. Short tandem repeat (STR) analysis of representative different cell lines. Related to Figure 1.

Table S2:

Dataset	Type	Cell type description	Raw data reads	Uniquely aligned reads(hg19)
UCF1	mRNA-seq	UCF	15,587,063	14,986,937
UCF2	mRNA-seq	UCF	12,886,105	12,351,277
hiHep1	mRNA-seq	hiHep	11,782,612	11,300,955
hiHep2	mRNA-seq	hiHep	11,793,071	11,315,088
hiHep3	mRNA-seq	hiHep	15,387,774	14,678,448
hiHep4	mRNA-seq	hiHep	13,777,553	13,136,450
iPSC-HLC1	mRNA-seq	iPSC-HLC	14,001,840	13,556,128
iPSC-HLC2	mRNA-seq	iPSC-HLC	14,152,516	13,703,578
iPSC-HLC3	mRNA-seq	iPSC-HLC	16,957,633	14,969,686
iPSC-HLC4	mRNA-seq	iPSC-HLC	16,159,800	15,616,574
PHH0d	mRNA-seq	PHH	13,627,191	13,060,672
PHH1d	mRNA-seq	PHH	16,068,468	15,277,617
PHH2d	mRNA-seq	PHH	15,455,998	14,720,381
PHH4d	mRNA-seq	PHH	13,989,274	13,391,254
H3k27ac_UCF1	Histone	UCF	23,634,469	19,500,077
H3k27ac_hiHep1	Histone	hiHep	24,147,889	21,664,019
H3K27ac_iPSC-HLC1	Histone	iPSC-HLC	20,296,814	16,848,508
Input_UCF1	Input	UCF	38,312,544	32,042,769
Input_hiHep1	Input	hiHep	27,152,133	22,888,166
Input_iPSC-HLC1	Input	iPSC-HLC	27,853,342	23,274,017

Table S2. Summary of data sets generated in this study. Related to Figure 2, Figure 4 and Figure 5.

Supplemental Experimental Procedures

Cell culture and generation of hepatocyte-like cells.

UCFs were cultured in human fibroblast medium (HFM), which is DMEM/F12 medium containing 10% FBS, 1% nonessential amino acids, 0.1 mM 2-mercaptoethanol, and 4 ng/ml bFGF. hiHep was generated from immortalized UCFs with transduction of *FOXA3*, *HNF1A* and *HNF4A*, and cultured in hepatocyte maintaining medium (HMM) as previously reported(Huang et al., 2014). iPSC-HLC was generated from iPSCs through a three-step method as previously reported(Szkolnicka et al., 2014). Briefly, iPSCs were maintained in mTeSR (Stemcell Technologies) on Matrigel (BD Biosciences). Before hepatic differentiation, iPSCs were passaged on Matrigel. At day 0-3, iPSCs were treated with RPMI/B27 plus Activin A (100 ng/mL) and Wnt3a (50 ng/mL). Then, in following 6 days, cells were cultured in SR/DMSO (DMEM/F12 containing 20% KOSR, 1 mM glutaMAX, 1% nonessential amino acids, 0.1 mM 2-mercaptoethanol, and 1% dimethyl sulfoxide [DMSO]). The final maturation step was culturing the cells in HepatoZYME medium (Life Technologies) supplemented with 0.5 × GlutaMAX, 10 μM hydrocortisone, 10 ng/ml HGF and 20 ng/ml OSM.

Primary human hepatocytes (PHH) from 3 individuals were purchased from Celsis In Vitro Technologies (Lot number: TLQ, FLO, YJM). Detailed information about the PHHs was provided in the product instructions. PHHs were pooled together at the same number and plated in the density of 1.25×10^5 /cm^2.

RNA extraction Polymerase Chain Reaction, PCR

For most experiments, total RNA was isolated from cells by Trizol (Invitrogen). For RNA extraction from formalin-fixed-paraffin-embedded (FFPE) tissues, RNA was extracted using RNeasy FFPE Kit (Qiagen).

A total of 1 μg RNA was reverse transcribed into cDNA with M-MLV Reverse Transcriptase (Promega) according to the manufacturer's instructions. Quantitative PCR (q-PCR) was performed with SYBR Premix Ex Taq (TaKaRa) on an ABI StepOne Plus real-time PCR system (Applied Biosystems). Primer sequences will be provided upon request. All q-PCR data were performed with at least 3 repeats.

Alkaline phosphatase staining and bisulfite genomic sequencing

The alkaline phosphatase activities of iPSCs were measured by Alkaline Phosphatase Kit (Sigma). For the methylation analysis of *OCT4* promoter regions, the genomic DNA of UCFs and iPSCs were collected and using CpGenome Turbo Bisulfite Modification Kit (Millipore) to measure their methylation levels.

Teratoma formation by human iPSCs

Feeder-free human iPSCs were collected by ReleSR treatment and injected subcutaneously into NOD-SCID mice. Teratoma were observed 1-2 months after injection and were collected typically in 2–3 months and processed for paraffin embedding and hematoxylin and eosin staining following standard procedures.

Flow cytometry analysis

For characterization of UCF by flow cytometry, UCFs were harvested and washed once in PBS solution (Gibco) with 1% BSA, and incubated with PE anti-human CD73 and APC anti-human CD 90 in dark for 30 min at 4 ℃. After incubation, cells were washed with PBS with 1% BSA twice and analyzed by the Calibur Flow Cytometer (Becton Dickinson). For analysis of HLCs, cells were harvested and washed once in PBS solution (Gibco) with 1% BSA, and then fixed by 4% PFA for 15 min and permeabilized by 0.3% Triton

X-100 for 15 min. After that, cells were incubated with ALBUMIN and α-1-antitrypsin (AAT) antibodies for 30 min at room temperature, and then incubated with the secondary antibodies for 15 min in dark at room temperature. After incubation, cells were washed twice and analyzed by the Calibur Flow Cytometer (Becton Dickinson). Antibodies for flow cytometry are as follows: PE anti-human CD73 (Biolegend 344003, 0.5μg/10^6cells), APC anti-human CD90 (Biolegend 328113, 0.5μg/10^6cells), mouse anti-Albumin (R&D mab1455, 2.5μg/10^6 cells), rabbit anti-AAT (NeoMarkers RB-367-A1, 1:200), goat anti-mouse IgG-PE (Santa Cruz sc-3738, 1:500), Alexa Fluor® 647-conjugated donkey anti-rabbit (Jackson Lab 711-605-152, 1:500). Data were analyzed with FlowJo software (Tree Star).

Immunofluorescent staining

For immunofluorescent staining, the cells were fixed with 4% paraformaldehyde for 15 min at room temperature, and then incubated with PBS containing 0.3% Triton X- 100 (Sigma) for 15 min. Cells were then washed three times with PBS. After being blocked by 3% BSA in PBS for 30 min at room temperature, cells were incubated with primary antibodies at 4 ℃ overnight, washed three times with PBS, and then incubated with appropriate fluorescence-conjugated secondary antibody for 30 min at room temperature in dark. Nuclei were stained with DAPI for 5 min.

Antibodies used for immunofluorescent staining are as follows: goat anti-human ALBUMIN (Bethyl Laboratories a80-229a, 1:100), mouse anti-human AFP (eBioscience 14-6583-80, 1:100), mouse anti-human SSEA4 (DSHB MC-813-70, 1:100), goat anti-human NANOG (R&D AF1997, 1:100), Cy3-conjugated donkey anti-goat IgG (Jackson Lab 705-165-003, 1:1000), Alexa Fluor® 647-conjugated donkey anti-mouse (Jackson Lab 715-605-150, 1:1000).

Human ALBUMIN and α-1-Antitrypsin ELISA

To determine the secretion of human ALBUMIN and α-1-Antitrypsin, supernatants of cell culture were collected after 48 hours culture from UCF, hiHep, iPSC-HLC. PHH were seeded on 12-well plates for 12 hours, and then maintained in HMM for 48 hours until collection of supernatants. Human ALBUMIN and α-1-Antitrypsin were measured by the human ALBUMIN ELISA Quantitation Set (Bethyl Laboratory) and the human α-1-Antitrypsin ELISA kit (Bethyl Laboratory) according to the manufacturer's instructions.

Assays for PAS, Oil Red O staining and UGT metabolism

For PAS staining, cells were stained by Periodic-Acid-Schiff (PAS, Sigma). Glycogen storage of UCF, hiHep, iPSC-HLC and PHH were determined by Glycogen Assay Kit (Abnova). For Oil Red O staining, confluent cells were stained by Oil Red O (Sigma-Aldrich), and quantitatively measured by counting oil numbers average to each cell. UGT metabolic abilities were measured by adding substrates to the supernatants and then measured by UGT Glo Assay Kit (Promega)

CYP induction, CYP metabolism and biliary excretion assay

For the measurement of CYP enzyme induction, UCF, hiHep, iPSC-HLC and PHH cells were cultured in HMM for 48 hours and then change to HMM supplemented with 3-methylcholanthrene (25μM), rifampicin (25μM) and sodium phenobarbital (2mM) for additional 48 hours.

For measurement of CYP metabolic activities, UCF, hiHep and iPSC-HLC were cultured for 6 days. On the experimental day, culture medium was removed, and hiHep cells were incubated with 5 μM testosterone (Sigma), the CYP3A substrate in 2 ml incubation medium. Cells were incubated on an orbital shaker for 0, 30,

60, 120, 240 min at 80-120 rpm for a 6-well plate. To stop the reaction, 300 μl cold methanol was added into 100 μl medium containing the substrate. The supernatants were collected for measurement of indicated productions by LC-MS/MS (LCMS-8030; Shimadzu, Kyoto, Japan). Plated cryopreserved hepatocytes were used as a positive control and UCF cells were used as a negative control.

D8-TCA and Rosuvastatin were analyzed by LC/MS/MS (LCMS-8030; Shimadzu, Kyoto, Japan). The amount of CLF was quantified by measuring fluorescence at 492 nm and 536 nm with a Synergy 4 microplate reader (Biotek, Winooski, USA). Biliary Excretion Index (BEI) was calculated as: BEI=(AHBSS-AHBSS(Ca^{2+} free))/AHBSS×100%.

Transplantation of UCF, hiHep, iPSC-HLC and PHH into FRG mice

Cells were intrasplenically transplanted into FRG mice after the withdrawn of NTBC water. Body weight was monitored twice a week post transplantation. Survived recipient mice were sacrificed to collect blood and liver samples 8 weeks after transplantation.

Histology and immunohistochemistry

Tissues were fixed overnight with 4% neutral formalin. Tissue sections were stained with haematoxylin and eosin for pathological evaluation. For immunohistochemical staining, paraffin sections (3-4 μm thick) were used. Slides were treated in 3% H_2O_2 for 15 min, blocked in 5% normal goat or horse serum in 1% BSA-PBS for 20 min, and stained with the indicated antibodies in 1% BSA-PBS overnight. Secondary antibodies were used according to Vectastain ABC kits (Vector Laboratories), followed by DAB staining (DAKO). FAH antibody (Cell Lab Tech, Inc. CLT602-910, Sunnyvale, CA) was used for immunohistochemical staining.

ChIP-seq data analysis

Raw reads were aligned by Bowtie (V1.1.1) (Langmead et al., 2009) against hg19 human reference genome with up to one mismatch. Then, non-uniquely mapped reads and PCR duplicates were removed. To generate the wig files, we extended the mapped reads to 200 bp. For further analysis, we normalized the read counts by computing RPKM (the numbers of reads per kilobase of bin per million of reads). Peaks of ChIP-seq samples were called by MACS(V1.3.7.1, parameter: -nomodel -nolambda) (Zhang et al., 2008) and weak peaks with p-value >=10e-40 were removed. The ChIP-seq data of Liver was downloaded from Roadmap Epigenomics and the GEO number of this data set is GSM1112808.

RNA-seq data processing

RNA-Seq datasets were mapped using TopHat2 (v2.0.13) (Kim et al., 2013) to the hg19 human reference genome. The mapped reads were further analyzed by Cufflinks(Roberts et al., 2011) and annotated using RefSeq database (Pruitt et al., 2012). The expression levels for each transcript were quantified by FPKM (Fragments Per Kilobase of transcript per Million mapped reads). For genes with multiple isoforms, the FPKM values were summed across all isoforms as the expression values for the genes. Differential expression analysis was carried out using the R (v.3.1.1) package DEseq (v.1.18.0) (Anders and Huber, 2010). Genes with Q value less than 0.01 and normalized more than 2 fold change were considered as differentially expressed genes. Heatmaps were constructed using R(v,3.1.1). Gene ontology analysis was performed using DAVID(v.6.7). Total RNA-seq data of RBE, Intestine, Endoderm and Liver progenitors were downloaded from (Forster et al., 2014; Loh et al., 2014; Sampaziotis et al., 2015; Yu et al., 2013) and mapped as described. The k-means clustering of gene expression levels at various samples were conducted using BICskmeans(Liu

et al., 2013).

Original data are available in the NCBI Gene Expression Omnibus (accession number GSE103078).

Supplemental References

Anders, S., and Huber, W. (2010). Differential expression analysis for sequence count data. Genome biology *11*, R106.

Forster, R., Chiba, K., Schaeffer, L., Regalado, S.G., Lai, C.S., Gao, Q., Kiani, S., Farin, H.F., Clevers, H., Cost, G.J., *et al.* (2014). Human intestinal tissue with adult stem cell properties derived from pluripotent stem cells. Stem cell reports *2*, 838-852.

Huang, P., Zhang, L., Gao, Y., He, Z., Yao, D., Wu, Z., Cen, J., Chen, X., Liu, C., Hu, Y., *et al.* (2014). Direct reprogramming of human fibroblasts to functional and expandable hepatocytes. Cell Stem Cell *14*, 370-384.

Kim, D., Pertea, G., Trapnell, C., Pimentel, H., Kelley, R., and Salzberg, S.L. (2013). TopHat2: accurate alignment of transcriptomes in the presence of insertions, deletions and gene fusions. Genome biology *14*, R36.

Langmead, B., Trapnell, C., Pop, M., and Salzberg, S.L. (2009). Ultrafast and memory-efficient alignment of short DNA sequences to the human genome. Genome biology *10*, R25.

Liu, Y., Qiao, N., Zhu, S., Su, M., Sun, N., Boyd-Kirkup, J., and Han, J.D. (2013). A novel Bayesian network inference algorithm for integrative analysis of heterogeneous deep sequencing data. Cell Res *23*, 440-443.

Loh, K.M., Ang, L.T., Zhang, J., Kumar, V., Ang, J., Auyeong, J.Q., Lee, K.L., Choo, S.H., Lim, C.Y., Nichane, M., *et al.* (2014). Efficient endoderm induction from human pluripotent stem cells by logically directing signals controlling lineage bifurcations. Cell Stem Cell *14*, 237-252.

Pruitt, K.D., Tatusova, T., Brown, G.R., and Maglott, D.R. (2012). NCBI Reference Sequences (RefSeq): current status, new features and genome annotation policy. Nucleic Acids Res *40*, D130-135.

Roberts, A., Pimentel, H., Trapnell, C., and Pachter, L. (2011). Identification of novel transcripts in annotated genomes using RNA-Seq. Bioinformatics *27*, 2325-2329.

Sampaziotis, F., Cardoso de Brito, M., Madrigal, P., Bertero, A., Saeb-Parsy, K., Soares, F.A., Schrumpf, E., Melum, E., Karlsen, T.H., Bradley, J.A., *et al.* (2015). Cholangiocytes derived from human induced pluripotent stem cells for disease modeling and drug validation. Nature biotechnology *33*, 845-852.

Szkolnicka, D., Farnworth, S.L., Lucendo-Villarin, B., and Hay, D.C. (2014). Deriving functional hepatocytes from pluripotent stem cells. Current protocols in stem cell biology *30*, 1G 5 1-1G 5 12.

Yu, B., He, Z.Y., You, P., Han, Q.W., Xiang, D., Chen, F., Wang, M.J., Liu, C.C., Lin, X.W., Borjigin, U., *et al.* (2013). Reprogramming fibroblasts into bipotential hepatic stem cells by defined factors. Cell Stem Cell *13*, 328-340.

Zhang, Y., Liu, T., Meyer, C.A., Eeckhoute, J., Johnson, D.S., Bernstein, B.E., Nusbaum, C., Myers, R.M., Brown, M., Li, W., *et al.* (2008). Model-based analysis of ChIP-Seq (MACS). Genome biology *9*, R137.